Delayed Stormflow Generation in a Semi-humid Forested Watershed Controlled by Soil Water Storage and Groundwater

Zhen Cui, Fuqiang Tian*

Department of Hydraulic Engineering, State Key Laboratory of Hydroscience and Engineering, Tsinghua University, Beijing 100084, China.

Corresponding author: Fuqiang Tian (tianfq@tsinghua.edu.cn)

Key Points:

- Threshold dynamics between soil water content and groundwater levels govern delayed stormflow generation. ~~Delayed stormflow is initiated when soil water content reaches field capacity.~~
- Groundwater fluctuations regulate the timing, magnitude, and merging of delayed and direct stormflow peaks. ~~Groundwater levels dictate the timing and magnitude of delayed stormflow.~~
- Hydrological connectivity and hydraulic conductivity increase with rising groundwater levels, driving delayed stormflow. ~~Rising groundwater levels enhance hydraulic conductivity and hydrologic connectivity, driving delayed stormflow.~~

Abstract

Recent research by Cui et al. (2024) identified a distinct threshold governing bimodal rainfall-runoff events in a semi-humid mountainous forested watershed in North China, ~~An analysis by Cui et al. (2024) of stormflow responses to rainfall in a mountainous forested watershed in the semi-humid regions of North China identified a distinct threshold for bimodal rainfall-runoff events,~~ where delayed stormflow appeared to be influenced by shallow groundwater dynamics. Building on these findings, ~~This~~ this study delves deeper into the mechanisms~~further investigates the processes~~ driving these bimodal events, focusing on the interactions~~dynamics~~ between ~~of~~ soil water content (SWC) and groundwater level (GWL) during storm events. The results show that delayed stormflow is primarily governed by the interplay between SWC and GWL. Delayed stormflow is initiated when SWC exceeds the soil's water storage capacity, while its timing and magnitude ~~volume~~further modulated ~~are determined~~ by GWL fluctuations. During rainfall, SWC increases rapidly but~~;~~ stabilizes after the rain ceases if ~~it does not reach~~ the soil's water-holding capacity is not reached~~, it stabilizes after the rainfall ends~~. Conversely, when~~if~~ SWC surpasses the ~~soil's~~ storage capacity, ~~it decreases rapidly post-rainfall, with~~ the excess rainwater infiltrates into the subsurface, recharging~~infiltrating deeper to recharge~~ groundwater~~,~~ and causing ~~leading to~~ a gradual rise in GWL. As GWL rises, enhanced~~increased~~ hydraulic conductivity facilitates the lateral movement of shallow groundwater toward ~~into~~ the stream channel, generating~~resulting in~~ delayed stormflow. Concurrently,~~Simultaneously,~~ the effective connectivity~~connection~~ ~~area~~ between the stream channel and adjacent hillslopes increases in the vertical dimension~~expands vertically~~. At ~~specific~~ higher GWL thresholds, GWL responses across the watershed become synchronized~~converge~~, significantly boosting~~increasing~~ groundwater discharge and reducing lag times~~,~~. In extreme cases,~~often causing~~ the delayed stormflow peak converges~~to merge~~ with the direct stormflow peak. These findings advance the understanding of delayed stormflow mechanisms in semi-humid mountainous watersheds, contributing to refining runoff generation theories by providing insights into the threshold-driven processes that govern the timing and volume of delayed stormflow.~~enhance our understanding of delayed stormflow generation in similar regions and contribute to refining runoff~~

generation theories.

Keywords: Delayed stormflow; Soil water storage; Groundwater outflow; Stormflow generation mechanism; Hydraulic conductivity

1. Introduction

Previous research on sStormflow processes in the Xitaizi Experimental Watershed (XEW), located in North China, exhibitidentified a frequent occurrence of bimodal stormflow hydrographs (Fig. A1), which often result inlead to significant stormflow and associated localized inundationflooding. Analysis of 15 such events over the past decade revealed thatOur findings highlighted that the onset of these bimodal hydrographs is governed by threshold behavior, . Specifically, with delayed streamflow peaks tend to emerging emerge when the combined total of event rainfall and antecedent soil moisture index exceeds 200 mm. Additionally, we The authors' findings suggest determined that shallow groundwater contributions are primarily responsible for these delayed stormflow events is primarily driven by contributions from shallow groundwater(Cui et al., 2024). However, the mechanisms underlying behind the development of these bimodal hydrographs, which represent complex emergent hydrological behaviors, remain poorly understood. UnderstandingGaining insight into the formation of delayed stormflow is crucial critical for advancing our comprehensionunderstanding of catchment runoff generation processes and improving flood forecasting capabilities.

Bimodal hydrographs, characterized by dual streamflow peaks,streamflow responses typically occur during the wetting-up phases of catchments. Extensive research has identified severalexamined the factors that influencing influence dual streamflow peaks, including revealing that bimodal hydrographs are associated with threshold behavior linked to antecedent soil moisture, antecedent precipitation, groundwater levels, soil water storage, and rainfall amount (Haga et al., 2005; Graeff et al., 2009; Anderson and Burt, 1978; Padilla et al., 2015; Martínez-Carreras et al., 2016). Despite these advancements,findings, the specific mechanismsreasons for suchthat lead to threshold behavior —and how these mechanisms produceit leads to the diverse shapes of stormflow hydrographs— are

still ~~remain~~ inadequately explained. For instance, Martínez-Carreras et al. (2016) ~~documented~~ found that a delayed peak only occurred when watershed storage reached a critical threshold of 113 mm. However, the precise reasons for this threshold and the underlying processes remain unclear~~that follow are not fully understood~~.

The occurrence of bimodal hydrograph reflects a ~~is a significant manifestation of the~~ nonlinear runoff response, which offers valuable insights into~~reflecting~~ the complex interactions between rainfall ~~runoff~~ and ~~rainfall~~runoff. ~~This n~~Nonlinear pattern ~~provides valuable insights into stormflow processes~~, including both the timing and magnitude of the response. Recent decades have seen an increase in research on nonlinear and threshold changes in rainfall-runoff responses, contributing to a deeper understanding of stormflow generation mechanisms. Nonlinear patterns~~shifts in stormflow~~, often characterized by rapid runoff responses that ~~can~~ may lead to flooding, have been extensively documented in recent decades (Detty and McGuire, 2010; Farrick and Branfireun, 2014; Graham et al., 2010; Tromp-van Meerveld and McDonnell, 2006a; Penna et al., 2011; Scaife et al., 2020). However, many studies fail to explore the intricate post-threshold mechanisms of these nonlinear shifts, leaving a gap in our understanding of stormflow generation across various catchments. While threshold behaviors are widely recognized, the detailed processes governing these shifts and their subsequent runoff dynamics remain underexplored. ~~However, much of the existing literature lacks detailed exploration of the intricate mechanisms that govern these shifts and the subsequent post-threshold runoff processes, leaving a gap in our understanding of these complex hydrological dynamics across diverse catchments.~~

Bimodal stormflow responses present an opportunity to investigate the relationship between rainfall thresholds and runoff generation, offering new perspectives on the timing and variability of stormflow.~~Bimodal runoff processes exemplify a typical nonlinear response of runoff, offering an intuitive and effective way to simplify the description of complex hydrologic systems.~~ Despite this, many studies fail to distinguish between unimodal and bimodal streamflow responses. For example, Detty and McGuire (2010) focused on hydrological threshold responses but did not differentiate between unimodal and bimodal hydrographs, as their study primarily addressed general nonlinear

rainfall-runoff processes in general. Similarly, Martínez-Carreras et al. (2016) observed delayed peaks but did not further classify streamflow responses due to their focus on overall watershed storage conditions. Such limitations often arise because the second peak in bimodal responses typically occurs after the rainfall event has ended, whereas many studies focus on streamflow changes during the event itself. Additionally, bimodal responses are influenced by catchment-specific topography and geology, making them less observable in certain regions. These challenges highlight the need for more in-depth investigation into bimodal streamflow responses to enhance our understanding of their mechanisms.~~Despite this, many studies fail to distinguish between unimodal and bimodal streamflow responses, limiting our understanding of these phenomena.~~ Therefore, an in-depth investigation into the mechanisms driving these responses is essential. Such research would enable the grouping of similar hydrologic responses and facilitate comparisons of stormflow generation processes across different watersheds (Graham and McDonnell, 2010; Tromp-van Meerveld and McDonnell, 2006a, b).~~–~~

Extensive studies across diverse regions have explored the role of soil water content and groundwater levels in generating delayed peaks in stormflow. Detty and McGuire (2010) emphasized subsurface flow thresholds in a forested catchment in the USA, while Farrick and Branfireun (2014) analyzed soil moisture and groundwater interactions in Canadian wetlands. Penna et al. (2011) examined antecedent soil moisture and storage thresholds in alpine catchments in New Zealand. These studies, along with others from regions such as Japan (Haga et al., 2005) and Europe (Graeff et al., 2009), contribute to the growing body of knowledge on threshold behavior in stormflow responses. However, while these studies highlight the occurrence of thresholds, the complex interactions that drive post-threshold runoff processes remain insufficiently understood.

Investigating~~Observing substantial~~ stormflow events in semi-humid regions, such as XEW, is challenging due to the relatively arid climate and low~~er~~ runoff coefficients. Over nearly a decade, 95 storm events were identified and analyzed in XEW, offering a rare and valuable dataset for examining bimodal stormflow responses in such regions.~~ Over the past decade, our analysis of 15 bimodal stormflow events has provided valuable data and insights, contributing to the advancement of runoff~~

~~generation studies in similar regions.~~ This study builds on prior findings to ~~focuses on the dynamics of SWC and GWL~~uncover ~~to investigate~~ the processes underlying delayed stormflow patterns. The primary objectives of this study are: (1) to analyze the temporal dynamics~~dynamics~~ of soil water content (SWC) and groundwater level (GWL) during storm events, (2) to elucidate the ~~intrinsic~~ mechanisms driving the threshold behavior observed in bimodal hydrograph ~~processess~~, and (3) to reveal the underlying processes responsible for~~generation mechanisms of~~ delayed stormflow ~~within~~ in ~~the Xitaizi Experimental Watershed~~XEW.

2. Materials and methods

2.1 Study site

The study was conducted in the Xitaizi Experimental Watershed (XEW), a 4.22 km² catchment located in North China (40°32′N, 116°37′E), ~~a small catchment in North China, located~~ approximately 70 km northeast of Beijing at ~~coordinates 40°32′N and 116°37′E~~ (Fig. 1). ~~XEW covers an area of 4.22 km², with~~The watershed's elevation~~s~~ ~~ranging~~ ranges from 676 to 1201 m above sea level, and the region experiences~~. The watershed is characterized by~~ a monsoon-influenced semi-humid climate~~, with an~~. The average annual precipitation ~~of~~ is 625 mm, with 80%~~80% of which~~ concentrated between~~occurs from~~ June and ~~to~~ September. The mean annual temperature is 11.5°C~~,~~ ~~and the~~ with an average relative humidity ~~is~~ of 59.1%. Forests cover 98% of the watershed, ~~dominated by~~with broad-leaved species and shrubberies accounting for ~~(~~54.2%~~)~~ ~~,~~and ~~–~~33.0%, respectively~~with coniferous and mixed forests comprising 2.3% and 10.5%, respectively. The catchment is heavily forested, with 98% coverage, comprising 54.2% broad leaved, 2.3% coniferous, and 10.5% mixed forests. Shrubs cover the remaining 33% of the land.~~

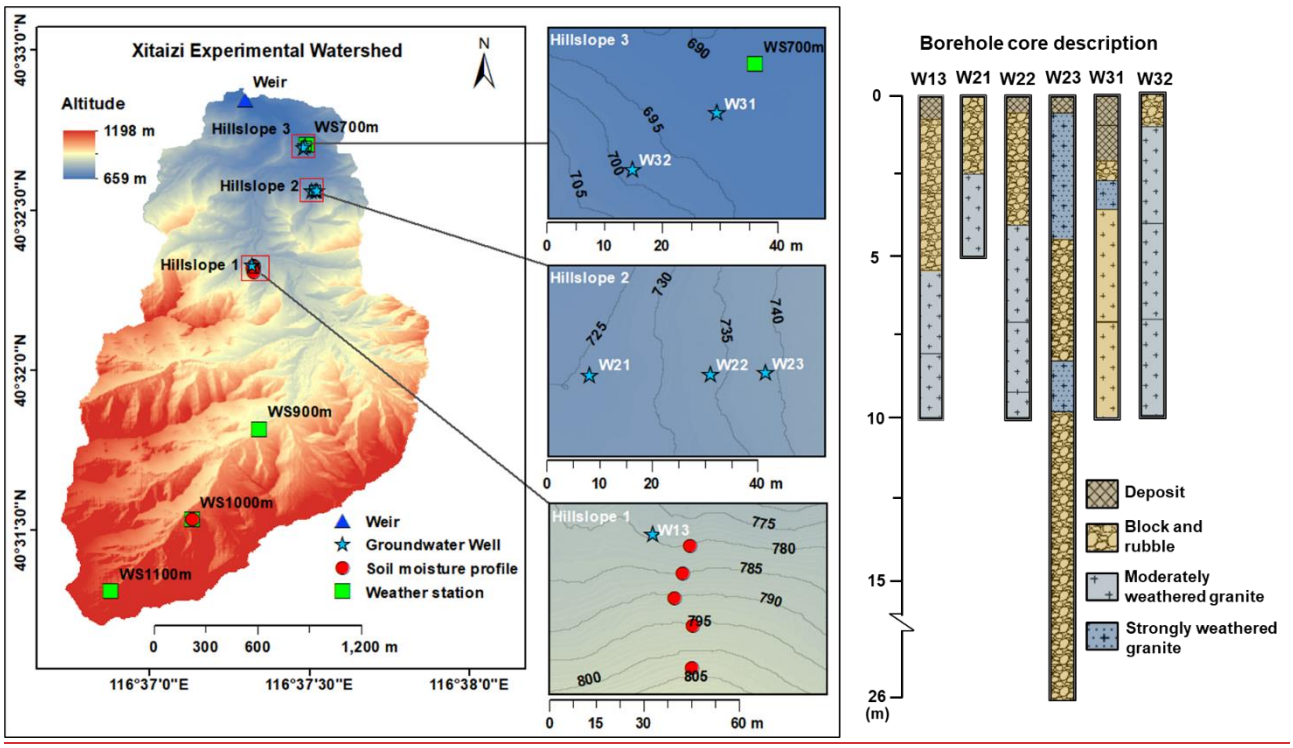
Xitaizi Experimental Watershed
Weir
Altitude
1198 m
659 m
Hillslope 3
WS700m
Hillslope 2
Hillslope 1
WS900m
WS1000m
WS1100m
Weir
Groundwater Well
Soil moisture profile
Weather station
0 300 600 1,200 m
116°37'0"E
116°37'30"E
116°38'0"E
40°33'0"N
40°32'30"N
40°32'0"N
40°31'30"N
N
Hillslope 3
690
W31
695
700
W32
705
0 10 20 40 m
Hillslope 2
730
725
735
740
W21
W22
W23
0 10 20 40 m
Hillslope 1
W13
775
780
785
790
795
800
805
0 15 30 60 m
Borehole core description
W13 W21 W22 W23 W31 W32
0
5
10
15
26
(m)
Deposit
Block and rubble
Moderately weathered granite
Strongly weathered granite

146

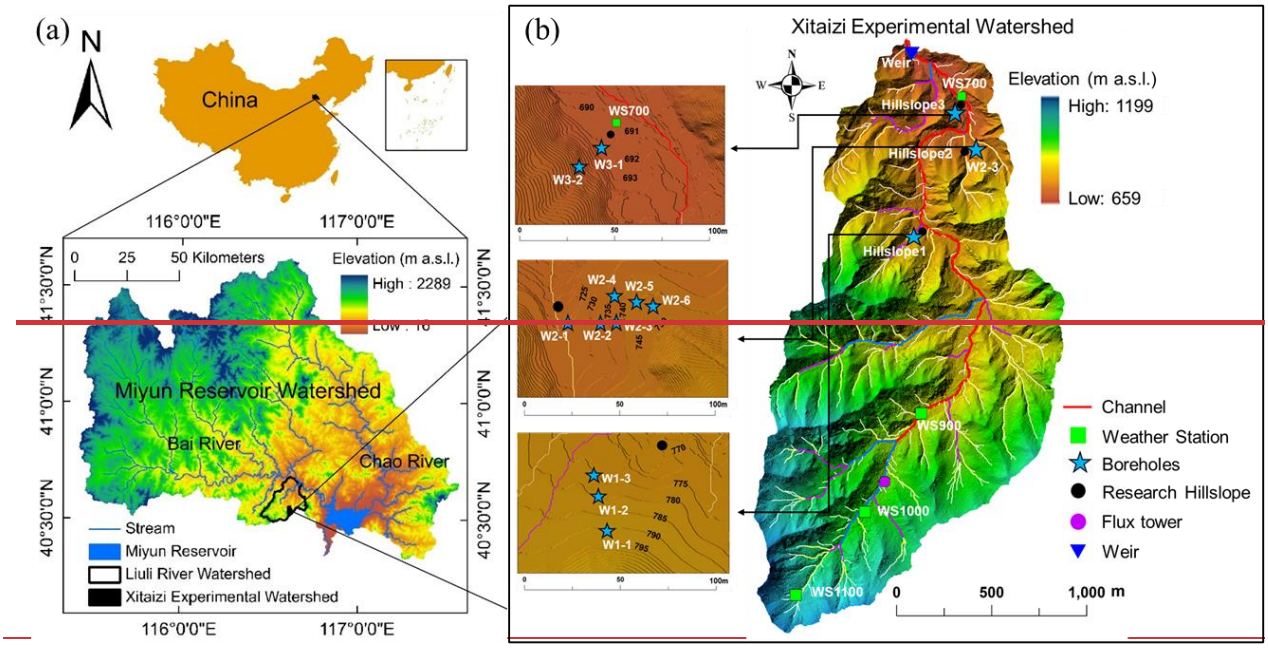
(a)
N
China
116°0'0"E
117°0'0"E
0 25 50 Kilometers
Elevation (m a.s.l.)
High : 2289
Miyun Reservoir Watershed
Bai River
Chao River
Stream
Miyun Reservoir
Liuli River Watershed
Xitaizi Experimental Watershed
41°30'0"N
41°0'0"N
40°30'0"N
(b)
Xitaizi Experimental Watershed
Weir
WS700
Hillslope3
Hillslope2
W2-3
Hillslope1
WS900
WS1000
WS1100
Elevation (m a.s.l.)
High: 1199
Low: 659
0 500 1,000 m
Channel
Weather Station
Boreholes
Research Hillslope
Flux tower
Weir
WS700
691
W3-1
692
W3-2
693
W2-4
W2-5
W2-6
W2-1
W2-2
W1-3
775
780
W1-2
785
W1-1
790
795

147

Figure 1. Location of Xitaizi Experimental Watershed (XEW) and a simple description of the borehole cores~~,~~. This figure shows the distribution of~~and the detailed distributed~~ monitoring ~~stations and~~ instruments, including four weather stations (WS700, WS900, WS1000, and WS1100), an outlet weir, ~~eleven~~six groundwater ~~boreholes~~ observation wells, and eight soil moisture observation profiles. Of the eight soil moisture profiles, five are located on Hillslope 1, while the remaining three are positioned on the slope near WS1000. Research hillslopes (Hillslope 1, Hillslope 2, and Hillslope 3) are delineated as key zones for hydrological and geological investigations. ~~and five soil water profiles.~~

The soils in XEW are primarily brown earth and cinnamon soils, with depths up to 1.5 m and an average saturated hydraulic conductivity of 45 mm/h. The surface soil is rich in organic matter, enhancing infiltration and reducing surface runoff potential. Underlying geology is predominantly compacted, deeply weathered granite (80% of the area), with smaller portions of gneiss and dolomite. Fractured granite facilitates vertical and lateral subsurface flow, contributing to delayed groundwater responses. Slug tests estimated the saturated hydraulic conductivity of weathered granite to range from~~The geology of XEW is dominated by firmly compacted, deeply weathered granite, accounting for approximately (80% of the catchment area.)The remaining bedrock consists of gneiss and dolomite. The saturated hydraulic conductivity of the weathered and fractured granite was estimated to range from~~ 5.2×10^{-3} m/day to 1.16 m/day ~~based on slug tests~~.

~~The watershed's soil types, primarily brown earth and cinnamon soil, extend to a depth of 1.5 meters with a saturated hydraulic conductivity ranging from 19.5 to 175.3 mm/h, averaging 45 mm/h.~~

2.2 Research hillslopes and instrumentation

Three research hillslopes (Hillslope 1, Hillslope 2, and Hillslope 3) were selected to investigate hydrological processes under varying geological and topographical conditions. Hillslope 1 (HS1) features thick soils overlying fractured granite, Hillslope 2 (HS2) has a highly permeable fractured block layer, and Hillslope 3 (HS3) consists of shallow soils over weakly weathered bedrock.

To capture spatial variability, SWC probes and boreholes were installed along hilltops, mid-slopes, and foot slopes. Groundwater boreholes, ranging from 5 to 26 m deep, were equipped with HOBO capacitance water level loggers to record GWLs (Fig. 1).

2.~~2~~ 3 Meteorological and streamflow~~hydrological~~ data collection~~measurements~~

Meteorological data spanning 2013–2023 were collected from four GRWS100 automatic weather stations (WS700, WS900, WS1000, and WS1100), positioned at elevations of 700, 900, 1000, and 1100 m, respectively. Rainfall was recorded at 10-minute intervals using six tipping-bucket rain gauges near the weather stations, and the data were averaged for analysis~~Meteorological data were collected from 2013 to 2023 using four GRWS100 automatic weather stations, strategically distributed along an elevation gradient within XEW (Fig. 1). Air temperature and relative humidity were monitored using HC2S3-L probes, equipped with radiation shields, while photosynthetically active radiation was measured with LI-190R quantum sensors. Rainfall was recorded at 10-minute intervals using six tipping-bucket rain gauges located in open areas near the weather stations, with data averaged for analysis~~.

Streamflow was measured at the catchment outlet using a Parshall flume, with water levels logged every 5 minutes since 2014. Data from some events were excluded due to sensor malfunctions or poor data quality, including key rainfall events in 2018 and 2019. Despite these exclusions, 95 rainfall-runoff events were analyzed, offering robust data for investigating bimodal stormflow characteristics.~~Streamflow was measured at the catchment outlet using a Parshall flume, with water levels recorded every 5 minutes by a HOBO capacitance water level logger from since 2014 onwards. The recorded data were averaged to hourly intervals for analysis. Due to environmental challenges, some data were lost, including stormflow data from July 19 to August 16, 2016, and streamflow data from 2018 to 2019, resulting in the exclusion of certain events from the analysis.~~

2.~~3~~ 4 Soil water content and groundwater level monitoring~~observation~~

Volumetric SWC was monitored at eight sites using CS616 time-domain reflectometry (TDR) probes installed at 10 cm intervals from the surface to 80 cm depth. Five profiles were located along HS1, and three were near WS1000. Measurements were recorded every 10 minutes, and the arithmetic mean of SWC values was used for analysis.~~Volumetric soil water content (SWC) was monitored using CS616 time-domain reflectometry (TDR) probes at eight locations within the watershed. Data were~~

~~recorded at 10-minute intervals, with five sensors installed on Hillslope 1 and three near WS900 at 80-cm depth intervals. For this study, the measurements were aggregated to hourly time steps, and the arithmetic mean SWC across the profiles was used for analysis.~~

~~2.4 Groundwater Level Observation~~

G~~roundwater level~~WLs (below the ground surface, hereinafter referred to as bgs) were observed in six boreholes distributed across the hillslopes. HOBO capacitance water level loggers recorded hourly data. To facilitate comparisons, GWLs were normalized using the method described by Detty and McGuire (2010). This normalization, expressed as the GWL index (I_G), standardizes GWLs across wells with varying ranges. ~~were observed in eleven 80-mm diameter boreholes distributed across three hillslopes within XEW (Fig. 1). Borehole depths ranged from 5 to 26 m, penetrating weathered and fractured granite with varying degrees of soil mantling. HOBO capacitance water level loggers recorded hourly groundwater levels. Boreholes W1-1, W1-2, W2-4, W2-5, and W2-6 frequently registered no water levels, potentially due to insufficient drilling depth. The saturated hydraulic conductivity of the weathered and fractured granite was estimated to range from 5.2×10^{-3} m/day to 1.16 m/day based on slug tests.~~

Groundwater levels were normalized ~~using an index (I_G) calculated for each borehole~~ following the method described~~approach~~ by Detty and McGuire (2010). For each well and event, the median height of the water table above the lowest recordable depth of the instrument was calculated and normalized to the total observed range, where 0 represents the minimum height and 1 represents the maximum height. This normalized value was referred to as the groundwater index (I_G). We used I_G to facilitate comparisons across wells with different absolute GWL ranges and to represent the overall GWL dynamics in the watershed.~~The arithmetic mean of IG across all boreholes was used to represent the overall groundwater level in the watershed.~~

Streamflow and SWC data were aggregated to hourly intervals for alignment with GWL data. Preliminary analysis confirmed that the delayed second streamflow peak had response times exceeding the hourly scale, rendering this aggregation sufficient for the study's purposes.

2.5 Rainfall-runoff event identification and hydrograph analysis ~~Separation of rainfall-runoff events~~

Rainfall events were identified using an intensity-based automatic algorithm described by Tian et al. (2012)~~. This algorithm~~ that defines event~~ start and end times based on a threshold~~ with rainfall intensity ~~of~~ >0.1 mm/h~~, with~~ and a minimum separation of six hours between events. ~~Only e~~Events with cumulative rainfall exceeding 5 mm were ~~included in the analysis~~analyzed~~, resulting in the identification of 95 distinct rainfall events from 2014 to 2023~~.

Bimodal rainfall-runoff events were manually identified based on two criteria: (1) the presence of a secondary, arch-shaped runoff peak occurring after rainfall cessation or during minimal intermittent rainfall, and (2) A distinct separation between the direct (sharp) and delayed (broad) peaks. More details of the classification are described in Cui et al. (2024, HESS).

The combination of automatic event delineation and manual identification ensured the accurate selection of 14 rainfall-runoff events with well-defined delayed peaks for subsequent analysis. Streamflow was separated into storm runoff and baseflow using the HYSEP program with the constant slope method (Hewlett and Hibbert, 1967; Sloto & Crouse, 1996), supplemented by manual adjustments for complex hydrographs. Event stormflow volumes were calculated as total discharge minus baseflow.

~~Storm runoff events were defined by a rapid streamflow increase and peak following rainfall. Streamflow hydrographs were separated into baseflow and stormflow components using the HYSEP program (Sloto & Crouse, 1996), with manual verification and adjustment based on straight-line separation principles.~~To quantify the runoff response, sStreamflow ~~hydrographs were~~was separated into ~~direct~~ storm runoff and baseflow ~~components. We utilized~~using the HYSEP computer program ~~(Sloto & Crouse, 1996), employing~~ with the constant slope method~~; Sloto & Crouse, 1996,~~ supplemented by manual adjustments for complex hydrographs~~.~~. Throughout the manuscript, stormflow refers to the total discharge, and event stormflow volumes were calculated as total discharge minus baseflow, which are expressed in q_s.

2.~~3~~ 6 Hydrological connectivity analysis~~Rainfall-runoff event analysis~~

Hydrological connectivity among streamflow, SWC, and GWL was analyzed to examine the interplay of subsurface flow pathways. Rainfall-runoff events were analyzed based on their total rainfall (>5 mm) and corresponding streamflow peaks. As illustrated in Fig. 2, The peak rainfall intensity (R_p) was determined based on the maximum 1-hour rainfall intensity, with the time of occurrence recorded as TP_p. Metrics such as initial streamflow (Q_0) and peak streamflow (Q_p) were determined alongside their respective timings (TQ_0 and TQ_p).~~The analysis focused onunderstanding the conditions under which subsurface flow connects to or disconnects from the stream. The dynamics among streamflow, SWC, and GWLs were examined to reveal connectivity patterns, providing insights into the underlying processes. This simultaneous observation of soil water, groundwater, and streamflow is defined as the soil water-groundwater–stream response relationship.~~

Similar metrics were calculated for SWC and GWL, including initial values (SWC_0 and I_{G0}) and peak values (SWC_p and I_{Gp}), with corresponding times of occurrence (TS_0, TI_{G0}, TS_p and TI_{Gp}). These metrics allowed for a comprehensive evaluation of the soil water-groundwater-streamflow response relationship across 95 distinct rainfall-runoff events.

~~Rainfall-runoff events, defined as those with total rainfall exceeding 5 mm and a corresponding peak in streamflow, were analyzed. The peak rainfall intensity (R_p) was determined based on the maximum 1-hour rainfall intensity, with the time of occurrence recorded as TP_p. the initial streamflow (Q_0) was defined as the streamflow just before it began to rise, and TQ_p was the time when the maximum streamflow (Q_p) occurred. TRs and TR_e represent the start and end times of rainfall, respectively. The analysis of SWC and GWL dynamics followed a similar approach to streamflow, replacing Q_0 and TQ_p with SWC_0 (I_{G0}) and TS_0 (TI_{G0}), and SWC_p (I_{Gp}) and TS_p (TI_{Gp}), respectively. This study analyzed 95 distinct rainfall-runoff events to better understand the interactions between soil water, groundwater, and streamflow in response to rainfall.~~

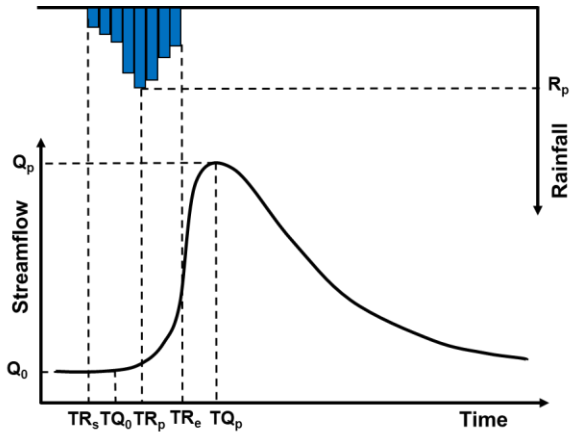

Figure 2. Definition sketch for analysis of rainfall event.

3. Results

3.1. Hillslope-scale dynamics of SWC and GWL during rainfall-runoff events ~~Relationship between SWC and GWL variability at the hillslope scale~~

The temporal evolution of ~~soil water content (~~SWC~~)~~ and ~~groundwater level (~~GWL~~)~~ was analyzed across 95 rainfall-runoff events to understand their dynamic interaction. Our analysis revealed a clear relationship between SWC and GWL dynamics, with SWC initially increasing rapidly during rainfall, followed by a stabilization or decline once a threshold was reached. In contrast, GWL showed a more delayed response (Fig. 3). Three distinct patterns of SWC and GWL interaction were identified ~~(Fig. 3):.~~ ~~We conducted a detailed analysis of the temporal evolution of SWC and GWL at the hillslope scale, focusing on their interactions across 95 rainfall-runoff events. Our analysis revealed a strong correlation between increases in GWL and elevated SWC values. During the early stages of these events, rainfall prompted a rapid rise in SWC, while GWL remained relatively stable. Once SWC reached a certain threshold, it either plateaued or gradually declined, coinciding with a marked increase in GWL. Subsequently, both SWC and GWL exhibited a nearly synchronous decline as GWL reached specific levels, manifesting in three distinct patterns of variation.~~

Figure 3 illustrates the dynamics ~~response characteristics~~ of SWC and GWL during three representative events. These events were selected to demonstrate the variability in SWC and GWL

patterns identified across the 95 rainfall-runoff events. The selected events all occurred within the same year to minimize inter-annual variability and ensure comparability. Red circles indicate rainfall periods ~~of rainfall~~, while black circles represent post-rainfall periods. In ~~a typical light rainfall event~~dry conditions,~~, as shown in Fig. 3a,~~ despite 66.6 mm of rainfall, SWC remained relatively low (<0.20), with a gradual increase during rainfall followed by stabilization after rainfall ceased. GWL showed minimal response.~~the soil remained relatively dry with SWC values mostly below 0.20. During rainfall, SWC increased steadily until the rainfall ceased, after which it stabilized, while GWL showed minimal change~~ (Fig. 3a).

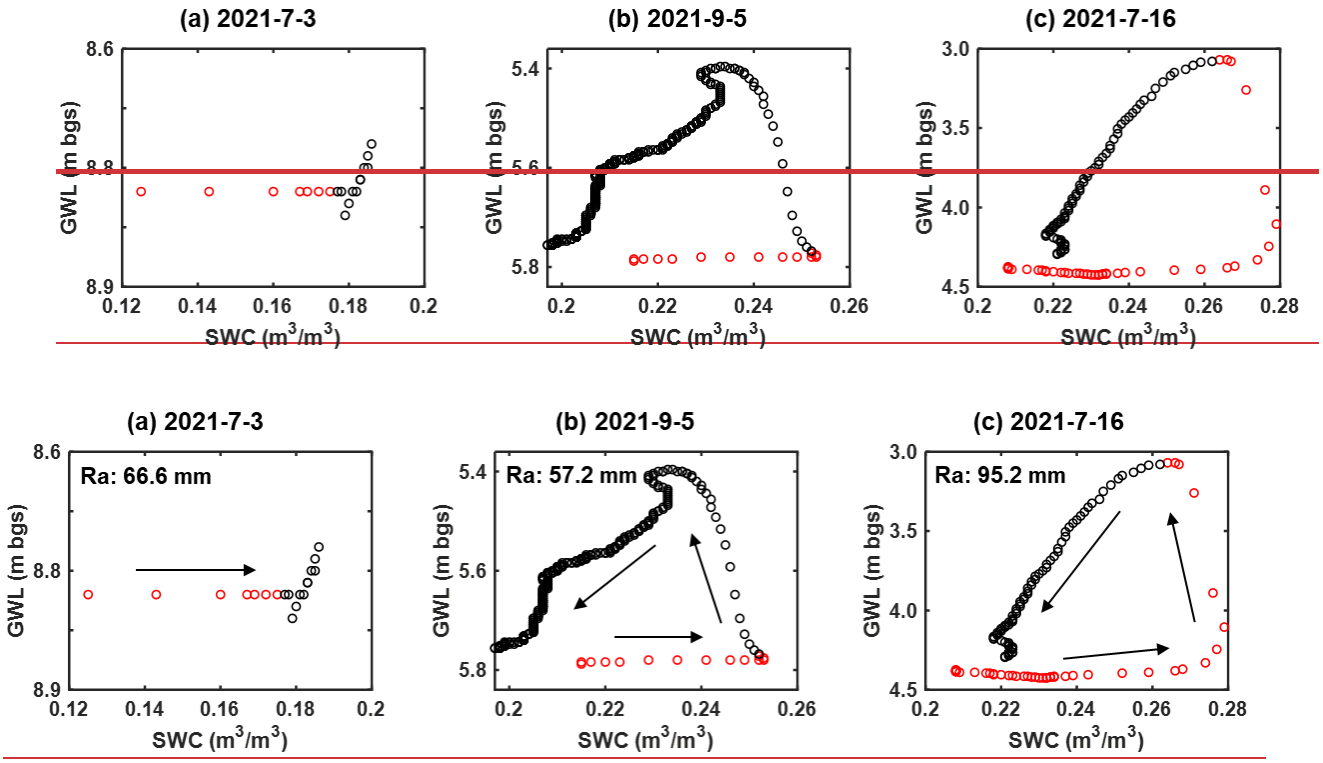

Figure 3. Three typical SWC-GWL dynamics patterns during rainfall-runoff events. Ra is rainfall amount. Arrows indicate the temporal evolution of the events. Red circles indicate periods of rainfall, while black circles denote post-rainfall periods.

In events with wet conditions, both SWC and GWL showed significant increases. However, the timing of GWL rise varied: in some cases, GWL rose after the cessation of rainfall, while in other cases, it began rising before the rainfall ended. ~~Figures 3b and 3c depict the dynamics of SWC and GWL during storm events, where a pronounced counterclockwise hysteretic relationship was~~

~~observed. Both SWC and GWL exhibited significant increases, with SWC surpassing 0.20.~~ The primary distinction between these patterns lies in the timing of the GWL rise: in Fig. 3b (57.2 mm rainfall), GWL began to rise after the rainfall ended, whereas in Fig.3c (95.2 mm rainfall), GWL started to rise noticeably before the end of the rainfall.

In the scenario represented by Fig. 3b, SWC increased significantly, surpassing 0.20, while GWL showed a delayed rise after the rainfall ceased. The counterclockwise hysteresis was observed as SWC continued to increase while GWL remained largely unchanged during rainfall.~~SWC continued to rise during rainfall while GWL remained largely unchanged. After the rainfall ceased, SWC began to decline, and GWL subsequently rose before eventually falling~~. Fig. 3c, which typically represents intense~~extreme~~ storm events, showed a sharp increase in both SWC and GWL, with SWC exceeding 0.25. GWL began to rise before the rainfall ended, reaching a peak as rainfall continued, and both variables showed a substantial decline after rainfall ceased.~~shows that when SWC exceeded 0.25, GWL rose sharply as SWC continued to increase until it reached 0.28. Despite ongoing rainfall, SWC then decreased, and GWL experienced a significant surge, continuing until the rainfall stopped, after which both variables began to decline.~~ These representative events highlight the variability in the SWC-GWL relationship, with timing differences in the rise of GWL and distinct hysteresis patterns during moderate and extreme events.~~This pattern underscores the complex dynamics of SWC and GWL during storm events, highlighting the nuanced responses of these hydrological parameters~~.

We further quantified the frequency distribution of SWC and GWL increases or decreases across the 95 rainfall-runoff events (Fig. 4). Notably, in 49 events, SWC increased, while GWL increased in 43 events. In contrast, SWC declined in 26 events and GWL declined in 15 events. Importantly, 15 events showed a simultaneous decline in both SWC and GWL, which were associated with delayed stormflow and larger stormflow volumes.~~As depicted in Fig. 4, there were 49 events where SWC increased and 43 events where GWL increased. Among these, 26 events saw a decline in SWC, and 15 experienced a decline in GWL, with only 15 events showing a decrease in both variables. These 15 events were associated with delayed stormflow and generated larger stormflow volumes.~~ One such event, on August 15, 2021, exhibited fluctuating SWC and GWL values throughout the rainfall event

due to the more dispersed rainfall distribution. As a result,~~Notably, the rainfall-runoff event on August 15, 2021, featured a more dispersed rainfall distribution, with multiple fluctuations in SWC and GWL throughout the event. Consequently,~~ our subsequent analysis primarily focused on the remaining 14 events with well-defined response characteristics.

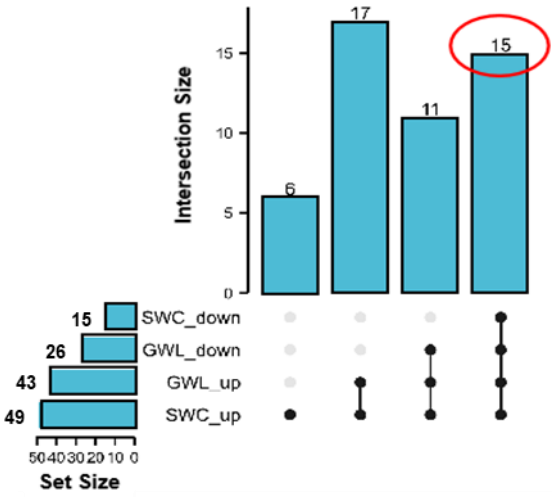

Figure 4. Upset plot of the response characteristics of ~~soil water content~~SWC and ~~groundwater level~~GWL~~–~~ during rainfall-runoff events ~~response characteristics~~.

3.2 SWC dynamics across rainfall-runoff events ~~Soil water content dynamics during storm events~~

Figure 5 presents the SWC dynamics observed during 14 distinct rainfall-runoff events, each characterized by minimal or no intermittent rainfall during the recession period. To facilitate a clear comparison of SWC changes across ~~different~~ events, the peak~~s~~ of ~~all~~ each event~~s~~ ~~were~~ was aligned ~~to the position corresponding to~~with a horizontal axis value of 0.

During the initial rainfall phase~~s of these events~~, SWC increased rapidly, reaching a peak value. As the rainfall ceased, SWC began to decline, though at a slower rate~~rainfall triggered a rapid increase in SWC, which quickly reached its peak. In the recession phase, the rate of SWC decline slowed as SWC decreased~~, eventually stabilizing ~~around~~ at a specific value. To quantify the threshold at which SWC stabilizes, we conducted a statistical analysis of the stable SWC during these events. The stable phase was defined as the period following the recession phase when SWC exhibited minimal variation

before subsequent rainfall. The statistical analysis of the stable SWC revealed a mean value of 0.1974, with a standard deviation of 0.0158 and a 95% confidence interval of [0.1945, 0.2003]. These results validate the visually observed threshold of 0.20 for SWC stabilization. ~~0.20. This~~ The general pattern of SWC variation is schematically illustrated~~represented~~ in Fig. 6.

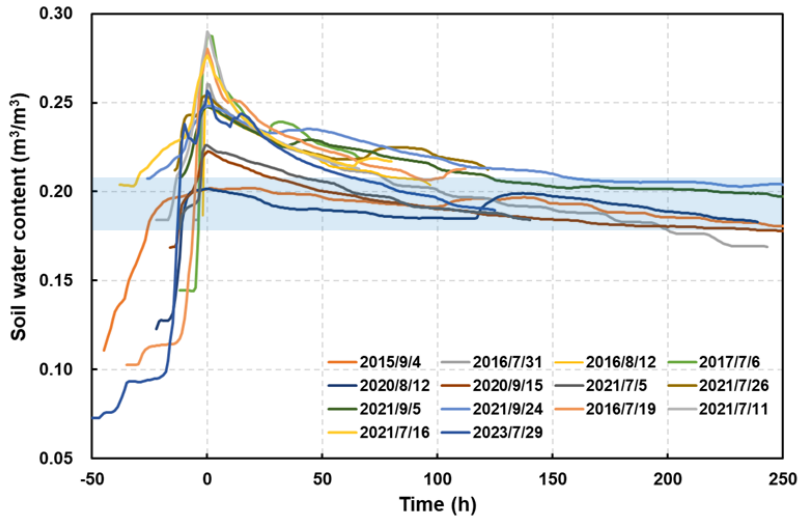

Figure 5. ~~Soil water content~~ SWC dynamics during ~~various~~different storm events.

The SWC response to rainfall ~~was found to be extremely~~is rapid. Upon rainfall ~~the~~ onset ~~of rainfall~~, SWC ~~quickly~~ increased sharply. Once the rainfall ceased, the subsequent behavior of SWC ~~was dependent~~ depends on whether the peak value exceeds the 0.20 threshold.~~its peak value~~. If SWC remains below or at~~was less than or equal to~~ 0.20, it either stabilize~~d for a period~~ or ~~decreased~~ declines ~~very~~ slowly. However, ~~if~~ when SWC ~~exceeded~~ exceeds 0.20, it decreased rapidly ~~,~~ ~~eventually~~before stabilizing around the 0.20 threshold. The magnitude of the peak above 0.20 influences the speed of the subsequent decline in SWC: the greater the peak, the faster the decline.~~The presence of a peak in SWC was determined by whether it surpassed the 0.20 threshold; the greater the excess above 0.20, the more rapid the subsequent decline.~~

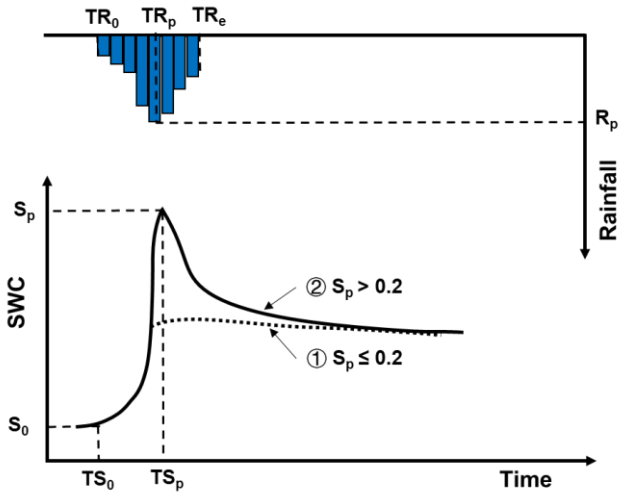

Figure 6. Schematic diagram of ~~soil water content~~SWC response ~~process~~ during storm events. S_p is the maximum SWC value ~~of soil water content~~.

3.3 GWL dynamics and response types~~during storm events~~

This section examines GWL dynamics during 14 selected rainfall-runoff events, chosen for their clear and consistent GWL and SWC patterns. These events facilitate a detailed investigation into groundwater response to storm events. ~~During storm events, w~~We identified two distinct GWL response types ~~of GWL responses:~~ quick and slow were identified~~. These response types~~ and are conceptually illustrated in Fig. 7. It is important to note that Fig. 7 is a schematic representation, not based on specific rainfall-runoff events, and does not include rainfall depth data.

~~The GWL with a quick response typically exhibits a distinct process curve compared to the slower response. The quick GWL response is closely aligned with a swift increase in soil water content (SWC), lagging the SWC peak by just 0 to 6 h (Fig. 7a). In scenarios where SWC exceeds 0.20, particularly beyond 0.24, the GWL often shows a secondary increase following its initial peak, marked by the dotted line in Fig. 7a. Conversely, a slower GWL response, depicted in Fig. 7b, occurs when SWC declines sharply after peaking.~~

~~Analysis of GWL variations across hillslope positions revealed that GWL in HS2 (W21-23) exhibits the rapid response type (Fig. 7a), while GWL in HS1 (W13) and HS3 (W31 and W32) demonstrates the slower response type (Fig. 7b). These response patterns suggest that the GWL~~

~~dynamics are not only influenced by SWC but are also dependent on the specific hillslope's geological structure.~~

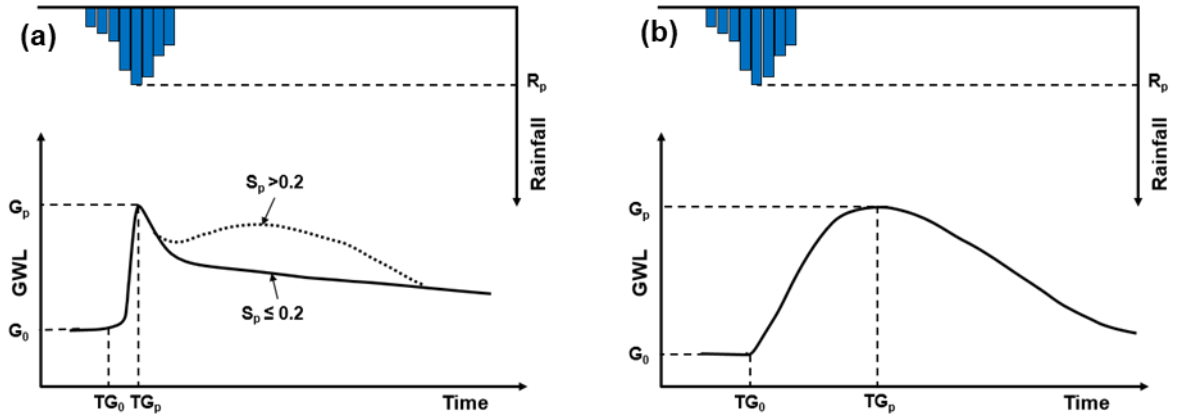

Figure 7. Schematic diagram of ~~groundwater level~~GWL response during storm events. G_0 and G_p represent~~are~~ the initial and maximum values of ~~groundwater level~~GWL, respectively. S_p ~~is~~ denotes the maximum SWC value ~~of soil water content~~.

In events exhibiting a quick response, the GWL rises rapidly, closely aligning with the SWC peak. The GWL response typically lags behind the SWC peak by 0 to 6 hours (Fig. 7a). For events where SWC exceeds 0.20 (and particularly when it surpasses 0.24), the GWL often shows a secondary rise following the initial peak, as indicated by the dotted line in Fig. 7a. Conversely, the slow response occurs when SWC declines sharply after reaching its peak, resulting in a delayed rise in GWL (Fig. 7b).

An analysis of GWL responses across various hillslopes revealed spatial variability. For instance, the GWL at HS2 (well W21-23) exhibited a quick response (Fig. 7a), whereas GWLs at HS1 (W13) and HS3 (W31 and W32) displayed slow response characteristics (Fig. 7b). These findings suggest that the GWL dynamics are influenced not only by SWC but also by the underlying geological structure of each hillslope.

At the watershed scale, ~~Further examination of GWL responses at various locations is presented in Fig. 8, which details the magnitude of GWL increases and the lag times relative to rainfall onset for each event. Despite variability in GWL across observation wells, with the exception of W21 and~~

~~W31 (which are located at the foot of the hillslope and exhibit smaller GWL changes), the differences in GWL increments at other wells are relatively minor, with mean increases ranging from 1 to 2 meters. On the same hillslope, GWL increments generally increase progressively from the foot to the top (e.g., W21, W22, and W23 on HS2, and W31 and W32 on HS3).~~GWL response to storm events demonstrated considerable spatial variability. I_G, represents the average normalized GWL across multiple wells, was used to capture an integrated view. Analysis revealed that I_G often exhibited two distinct peaks during storm events. Among the 14 events analyzed, 9 events displayed dual I_G peaks, coinciding with the two peaks in streamflow. However, at the individual well level, only W13 (HS1) and W23 (HS2) exhibited dual GWL peaks. Specifically, W13 showed two peaks during one event, while W23 exhibited two peaks during five events. The remaining wells displayed only a single peak across all events analyzed (see Table 1).

Table 1. Statistical results of response characterization of streamflow, I_G and groundwater levels.

			HS1	HS2			HS3	
	Streamflow	**I_G**	**W13**	**W21**	**W22**	**W23**	**W31**	**W32**
Total number of events	14	14	14	8	14	14	9	9
Number of events with two peaks	9	9	1	0	0	5	0	0

3.4 GWL responses across hillslope positions

Further examination of GWL responses across various locations is presented in Fig. 8, which shows the magnitude of GWL increases and their lag times relative to rainfall onset. While variations in GWL were observed among the monitoring wells, the differences in GWL increments were generally modest, with mean increases ranging from 1 to 2 meters. Notably, smaller GWL changes were recorded at the foot of the hillslope (e.g., W21 and W31). Within the same hillslope, GWL increments tended to increase progressively from the foot to the top, as seen in HS2 (W21-W23) and HS3 (W31 and W32).

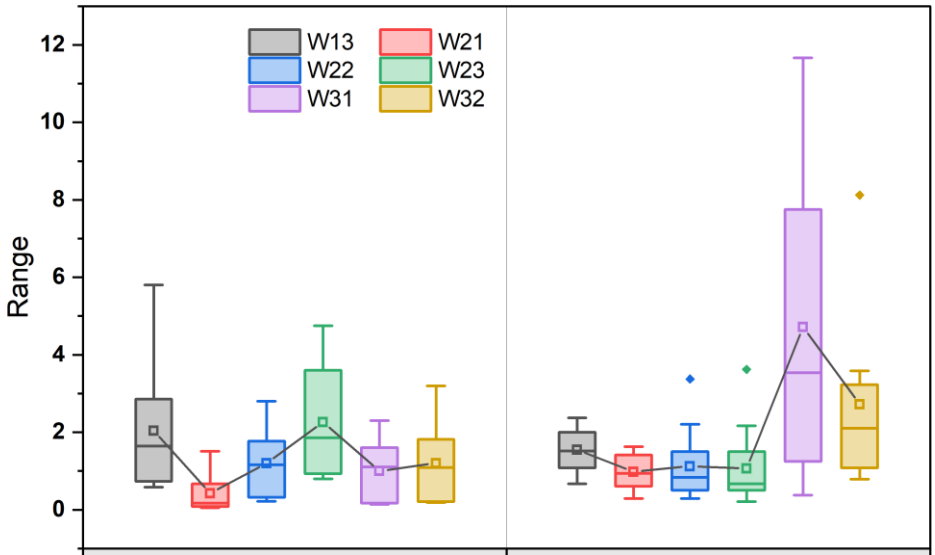

	ΔGWL (m)						Lag time (day)					
Location	W13	W21	W22	W23	W31	W32	W13	W21	W22	W23	W31	W32
Min	0.6	0.1	0.2	0.8	0.1	0.2	0.7	0.3		0.2	0.4	0.8
Max	5.8	1.5	2.8	4.8	2.3	3.2	2.4	1.6	3.4	3.6	11.7	8.1
Mean	2.0	0.4	1.2	2.3	1.0	1.2	1.5	1.0	1.1		4.7	2.7

Figure 8. ~~Groundwater level~~GWL increments (ΔGWL) and lag time of peak ~~water level~~GWL relative to rainfall onset at different~~across~~ locations.

In contrast, the~~However,~~ lag times for ~~reaching~~ maximum GWL exhibited greater variation across locations. For instance, at HS3, lag times ranged from 0.4 to 11.7 days ~~the delay for maximum GWL in~~at W31 ~~ranged from 0.4 to 11.7 days,~~ and from 0.8 to 8.1 days ~~in~~ at W32, ~~from 0.8 to 8.1 days,~~ significantly ~~both of which are~~ longer than those~~the lag times observed~~ at HS1 (0.7 to 2.4 days) and HS2 (0.2 to 3.6 days). Interestingly, within a single hillslope, ~~There is~~ no consistent relationship~~clear correlation~~ was found between the lag time of maximum GWL and its distance from the ~~hillslope~~ foot of the hillslope~~within the same hillslope~~. ~~These discrepancies in lag times between different hillslopes may be attributed to spatial variations in geological conditions, as suggested by Kosugi et al. (2011) and Padilla et al. (2015).~~

To further investigate these dynamics, the relationship between GWL increments and SWC was analyzed across 14 storm events (Fig. 9). The analysis focused on six observation wells (W13, W21–W23, W31, and W32) located on three hillslopes (see Fig. 1 for well locations). The variability in GWL response types—quick versus slow—was attributed to spatial differences in SWC thresholds

and hillslope geological structures.

~~Figure 8 reveals that while the magnitude of GWL increments across various locations remains relatively consistent, the lag time for GWL to reach its maximum value exhibits substantial variation. To further investigate these dynamics, we analyzed the relationship between GWL increments and SWC across 14 storm events. In Fig. 9, the length of the orange bar represents the GWL increment during the phase when SWC increased to its peak, while the green bar indicates the GWL increment during the phase when SWC decreased from its peak until GWL reached its maximum. The black and red dotted lines mark the initial SWC and the SWC at the onset of GWL rise, respectively. Locations without bars in Fig. 9b, e, and f indicate missing data.~~

~~The analysis shows that a significant increase in SWC from its initial value following rainfall is indicative of a delayed GWL response. Specifically, the larger the difference between the SWC at the onset of GWL rise (SWC_G) and the initial SWC (SWC_0), the later the GWL rise begins. Conversely, if SWC_G and SWC_0 are closely aligned, the GWL begins to rise almost simultaneously with the increase in SWC.~~

~~For example, at HS1 (W13), GWL began to rise only after SWC exceeded 0.20, and the majority of the GWL increase occurred during the SWC decline phase. This suggests that the GWL response on HS1 is influenced by soil wetness, indicating a potential threshold effect of SWC on GWL dynamics. On HS2 (including W21-23), the GWL response was more immediate, with increases closely following SWC rises. Here, the SWC at the onset of GWL rise varied widely, ranging from 0.13 to 0.26, and was generally close to the initial SWC, suggesting that GWL increases at these locations are less dependent on SWC thresholds. HS3 exhibited both quick and slow GWL responses. The initial response occurred soon after the SWC increase but at a slow rate that persisted over an extended period. The majority of the GWL increment at HS3 occurred during the SWC decline phase after its peak.~~

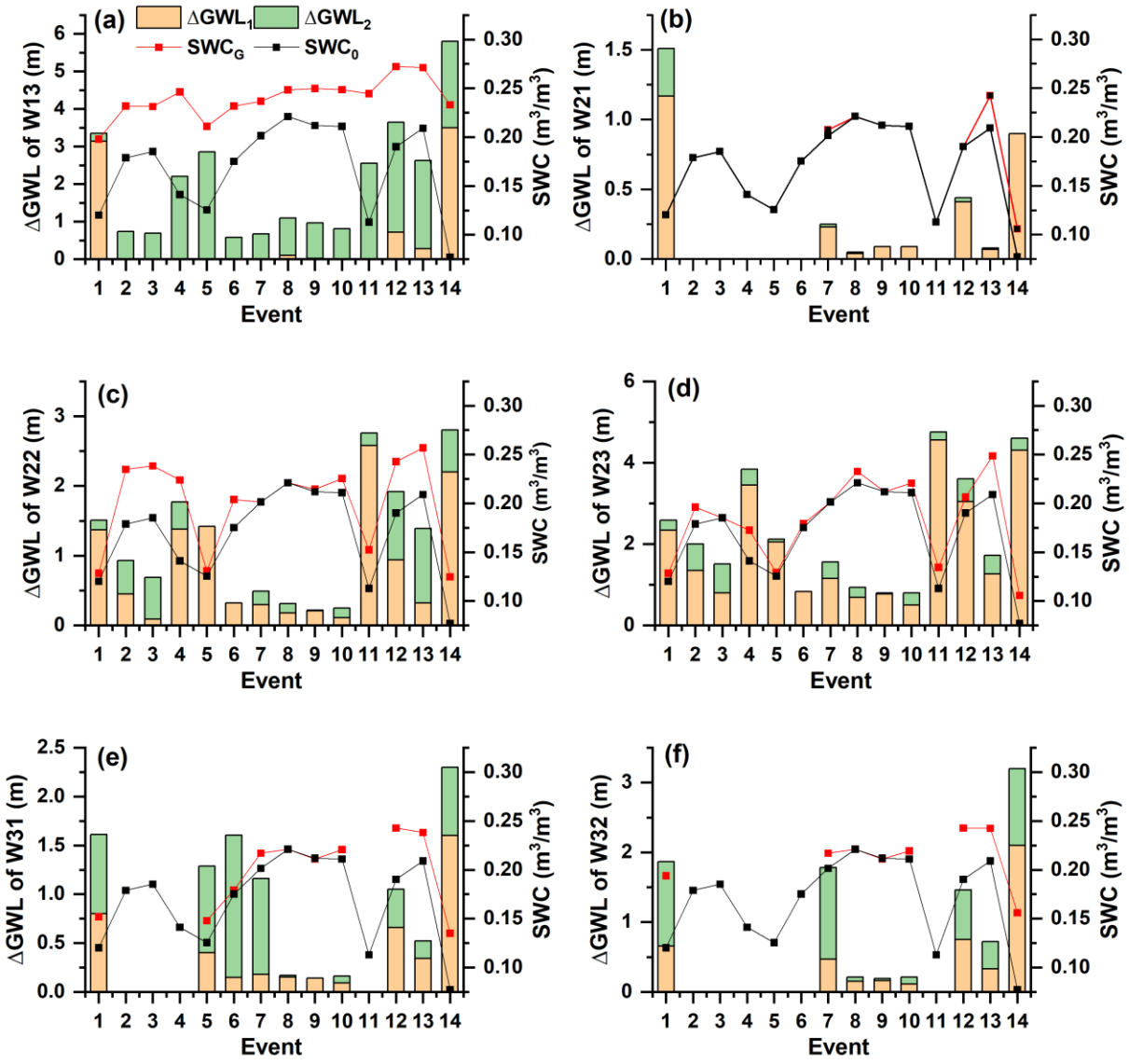

Figure 9. ~~Groundwater level~~GWL increments (ΔGWL) across various locations during 14 storm events, along with initial ~~soil water content~~SWC (SWC_0) and ~~corresponding soil water content~~SWC at the onset of GWL rise~~groundwater level initiation~~ (SWC_G). The orange bars represent ΔGWL during the SWC increase phase, while the green bars represent ΔGWL during the SWC decline phase. The red and black lines denote SWC_G and SWC_0, respectively.

In Fig. 9, the orange bars represent GWL increments during the SWC increase phase (up to its peak), while the green bars indicate GWL increments during the SWC decline phase (from its peak to when GWL reached its maximum. The black and red dotted lines mark the initial SWC (SWC_0) and the SWC at the onset of GWL rise (SWC_G), respectively. Missing data for some locations are indicated by the absence of bars in Figs. 9b, 9e, and 9f.

The analysis revealed that the magnitude of the SWC increase following rainfall onset is a key determinant of delayed GWL responses. Specifically, a greater difference between SWC_G and SWC_0 corresponded to an onset of GWL rise begins. Conversely, when SWC_G and SWC_0 are similar, GWL rose almost simultaneously with the SWC increase.

At HS1 (W13), GWL began to rise only after SWC exceeded 0.20. Most of the GWL increase occurred during the SWC decline phase, suggesting that soil wetness exerts a threshold effect on GWL dynamics. This delayed response aligns with the slow response type. At HS2 (W21-23), GWL responses were more immediate, with GWL increases closely following SWC rises. SWC_G values at these locations ranged widely (0.13-0.26) but were generally close to SWC_0, indicating that GWL responses at HS2 are less dependent on SWC thresholds and exhibit a quick response type.

HS3 demonstrated both quick and slow GWL responses. Initial rises occurred soon after the SWC increase, but the majority of GWL increments took place during the prolonged SWC decline phase following its peak. This pattern suggests a more complex interaction of immediate and delayed factors influencing GWL dynamics at HS3.

Thesese findings highlightindicate a strong relationship betweenthat the emergence of quick and slow GWL response types is strongly linked toand SWC dynamics. In quick response types, GWL growth increments occur primarily occurs during the SWC increase phase, resulting in a steep response curve. In slow response types, GWL growth increments predominantly predominantly occur occurs during the SWC decline phase after the peak, leading toproducing an arch-shaped response curve. This These distinctions underscores the pivotal critical role of SWC dynamics in regulatinggoverning the timing and magnitude of GWL responses across different hillslopes.

3.43.5 Characterization of groundwater response at the watershed scale

Figure 11 10 illustrates the timing of I_G peaks relative to the soil water content (SWC) response. The first I_G peak occurred rapidly following rainfall, initiating 0-2 h after the SWC began to rise and reaching its and peaking peak occurring 0-9 h later (average mean: 3.7 h) after the SWC reached its

maximum. In contrast, ~~The~~ the second I_G peak typically occurred post-rainfall, lagging behind ~~behind~~ the SWC peak by 10-65 h (~~average~~ mean: 28 h). These ~~response~~ patterns align with~~are consistent with~~ the quick and slow GWL response types identified in section 3.2. The occurrence of dual ~~occurrence of two~~ I_G peaks ~~is~~ can be~~primarily~~ attributed to the superimposition of groundwater contributions from different hillslopes~~, each~~ with differing~~distinct~~ response rates. The first (quick) ~~fast~~ GWL response is tightly coupled ~~closely linked~~ to ~~immediate~~ rainfall onset and ~~rising~~ SWC increases, while~~whereas~~ the second (slow)~~slow~~ GWL response reflects gradual infiltration and groundwater recharge occurring~~occurs~~ over a broader timescale~~, emphasizing the need for further attention to the latter in hydrological studies~~.

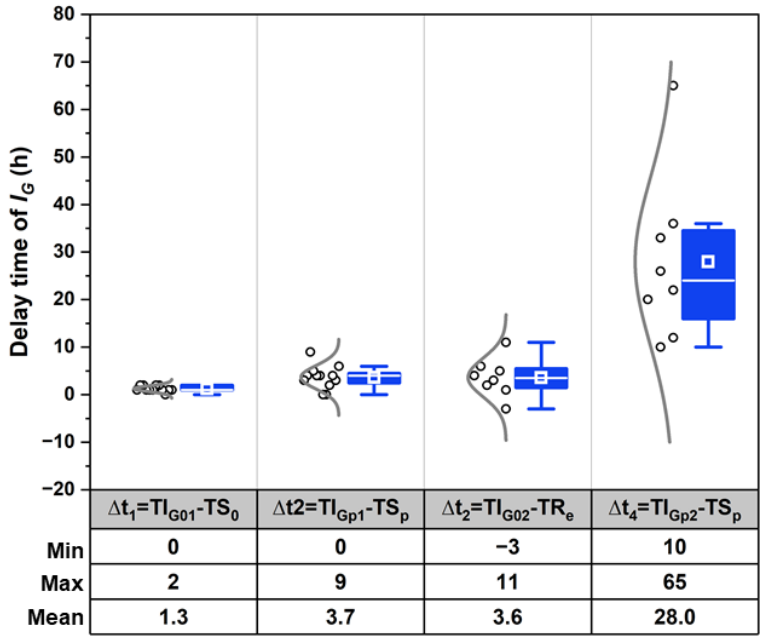

	Δt_1=TI_{G01}-TS_0	$\Delta t2$=TI_{Gp1}-TS_p	Δt_2=TI_{G02}-TR_e	Δt_4=TI_{Gp2}-TS_p
Min	0	0	−3	10
Max	2	9	11	65
Mean	1.3	3.7	3.6	28.0

Figure ~~11~~10. Delay time of I_G peaks relative to peak ~~soil water content~~SWC. TI_{G01} and TI_{G02} represent~~are~~ the onset times of the first and second peaks of I_G, respectively. TS_0 and TS_p indicate~~are~~ the time when ~~soil water content~~SWC started to increase and peaked, respectively. TI_{Gp1} and TI_{Gp2} represent~~are~~ the time when I_G started to increase and peaked, respectively. TR_e indicates ~~is when~~ the end of rainfall ~~ends~~.

The growth rates of I_G towards the two peaks ~~in various events~~ were also quantified (Fig. ~~12~~11). A notable disparity was observed between the growth rates of the first (r_1) and second (r_2) ~~two~~ I_G peaks~~, . with the~~ The first I_G peak ~~(r_1)~~ exhibited~~displaying~~ a ~~significantly higher~~ markedly faster

rates (0.03 to 0.98/day, mean: 0.38/day) compared to ~~than~~ the second peak (0.01 to 0.31/day, mean: 0.07/day) ~~(r_2)~~. ~~Specifically, r_1 ranged from 0.03 to 0.98 per day (average 0.38/day), while r_2 ranged from 0.01 to 0.31 per day (average 0.07/day).~~ These differences reflect~~two peaks correspond to~~ the contrasting dynamics of quick and slow GWL responses across ~~different~~ hillslopes. In events featuring dual~~two~~ I_G peaks, the maximum I_G was typically ~~occurred~~ observed at the second peak. However, ~~Additionally, i~~in events ~~characterized by~~with higher GWLs (indicating lower I_G), the ~~disparity~~difference between the growth rates ~~of the two I_G peaks~~ diminished, making the two peaks harder ~~them more difficult~~ to distinguish ~~, as observed in~~(~~e~~e.g., Events 9 and 10). In ~~events~~ Events 11-14, w~~hich had much higher~~ here GWLs were significantly higher,~~,~~ only a single I_G peak was observed ~~in the I_G process~~. ~~This outcome aligns with the findings presented in Fig. 10, indicating that higher GWLs lead to a more synchronized GWL response across the watershed.~~

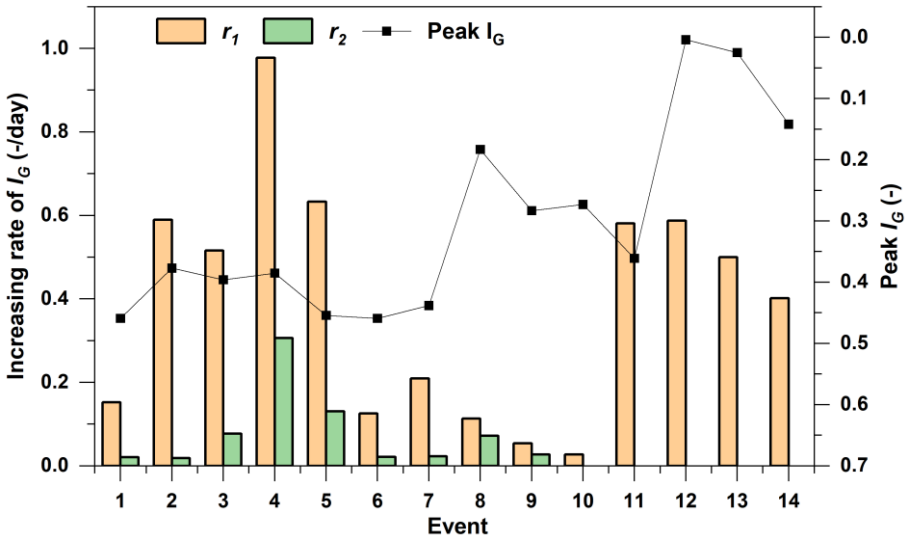

Figure ~~12~~11. Growth rates of I_G and ~~its~~ the maximum I_G value across storm ~~various~~ events. r_1 and r_2 denote the ~~rates of~~ ascent rates during ~~the periods when I_G reaches its~~the first and second peaks, respectively.

The contrasting dynamics of the two IG peaks highlight their distinct formation mechanisms. The first I_G peak, ~~which~~ occurr~~ed~~ing ~~rapidly~~ during rainfall, ~~and was~~is closely associated with the rapid rise ~~rising~~ in SWC~~,~~. Conversely,~~contrasts with~~ the second I_G peak emerges~~, which appeared~~ post-rainfall, coinciding with soil~~when the soil layer began~~ draining and groundwater recharge processes. ~~The formation processes and underlying mechanisms of these two I_G peaks are distinct.~~ As

reported by Dang et al. (2023) ~~noted~~, rainfall induces~~generates~~ pressure waves that rapidly expel soil water from the lower soil column~~'s bottom~~, while infiltrated rainwater migrates downwards at slower ~~pacely downward~~. pressure-driven displacement generates a near-instantaneous~~This change in head within the surface soil layer can induce an immediate~~ GWL response during the initial phase of rainfall.

We hypothesize that the ~~fast~~ rapid I_G peak ~~may result from increased SWC inducing a~~is linked to kinematic wave triggered by increased SWC, which displaces pre-existing "old" soil water and groundwater ~~ahead~~, leading to a synchronized ~~near-synchronous~~ GWL rise (e.g., Anderson and Burt, 1978). Despite~~Although~~ the slow percolation of water ~~water flow~~ through soil and bedrock ~~is slow~~, the theoretical celerity of this kinematic response is near-~~response is~~ instantaneous, accounting for ~~hence~~ the rapid GWL ~~GWL~~ rise. Furthermore, ~~early~~ drilling data suggest that ~~revealed~~ the presence of faults in the ~~rock structure~~bedrock of HS2, potentially facilitating~~which may contribute to the~~ faster groundwater~~GWL~~ response on this hillslope compared to others.

The second, slow I_G peak is likely ~~forms~~ driven by the ~~as rainwater~~ gradual~~ly~~ ~~infiltrates~~ infiltration of rainwater ~~through the~~into deeper soil and bedrock layers, ~~eventually~~ ultimately recharging the groundwater. This process is regulated by the soil's water storage threshold. B~~Crucially, there exists a threshold for the soil layer's water storage capacity: b~~efore reaching this threshold,~~SWC reaches this threshold,~~ the soil retains all incoming rainfall. Once exceeded, excess water drains rapidly into~~all rainfall is retained within the soil layer. Once this critical threshold is surpassed, the soil layer cannot retain additional water for extended periods and swiftly releases excess water to~~ deeper layers, leading to a ~~subsequent~~ decline~~reduction~~ in SWC and a concurrent rise in~~while the~~ GWL ~~rises~~ due to ~~effective~~ groundwater ~~replenishment from infiltrated rainwater~~recharge.

4. Discussion

4.1 Inter-hillslope GWL dynamics

GWL variations in lag times and response magnitudes across hillslopes can be attributed to

differences in geological conditions. HS1 and HS3 are primarily underlain by fully to strongly weathered granite, with upper layers comprising significant soil-rock mixtures. These features lead to relatively slower GWL responses, likely due to the limited permeability of the regolith and underlying materials. In contrast, HS2 is characterized by a fractured rock layer at depths of 10-30 meters (see Fig. 1), which enhances subsurface flow and facilitates faster GWL responses. These geological contrasts explain the observed differences in GWL response times among the hillslopes.

Among the three hillslopes, HS3 exhibited the slowest GWL responses, characterized by the longest lag times. This distinct behavior makes HS3 a crucial reference for understanding inter-hillslope variations in GWL dynamics. Previous study by Cui et al. (2024) highlighted that GWL response times are closely linked to delayed stormflow timing, emphasizing the importance of examining GWL dynamics. Comparing the GWL response times of HS1 and HS2 with those of HS3 provides insights into how geological structures and SWC thresholds influence delayed stormflow generation.

Furthermore, the deeply weathered regolith and extensive fracturing in HS2 promote more rapid stormflow generation, as water stored in the regolith layer contributes to streamflow over extended periods. This finding aligns with previous studies (Kosugi et al., 2011; Padilla et al., 2015), which demonstrated that geological features such as fracture density and weathering depth influence subsurface flow paths and, ultimately, groundwater dynamics.

To deepen understanding of the inter-hillslope differences in GWL responses, we calculated the lag times between rainfall onset and peak GWL responses for all observation wells on each hillslope, incorporating spatial variability. Average lag times, denoted as t_{S1}, t_{S2} and t_{S3} for HS1, HS2, and HS3, respectively, were used to calculate the time differences $\Delta t = t_{S1} - t_{S3}$ and $\Delta t = t_{S2} - t_{S3}$. These time differences were then analyzed for their correlation with I_G, as illustrated in Fig. 12.

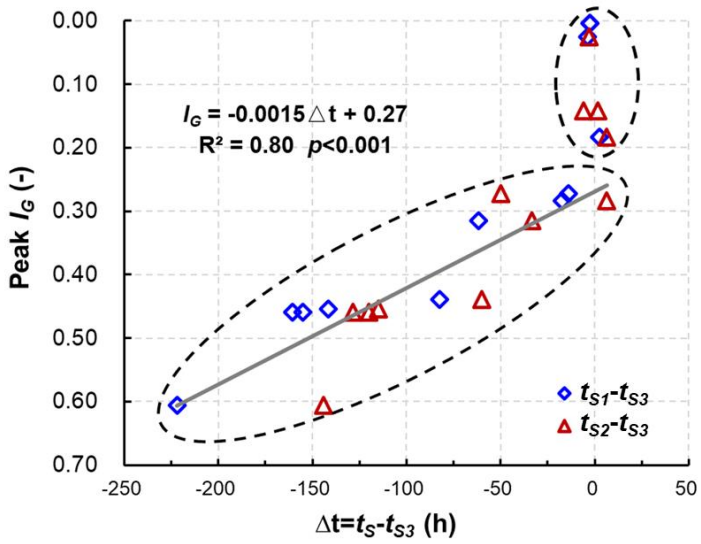

Figure 12. Correlation between peak I_G and the time differences from peak GWL responses on HS1, and HS2 to HS3 ($\Delta t=t_S-t_{S3}$), where t_{S1}, t_{S2} and t_{S3} are the average lag times of peak GWLs on HS1, HS2 and HS3, respectively.

In Fig. 12, blue diamonds represent $\Delta t = t_{S1} - t_{S3}$, while red triangles represent $\Delta t = t_{S2} - t_{S3}$. Both pairs exhibit a significant negative correlation with peak I_G, described by the equation: $I_G = -0.0015 \times \Delta t + 0.27$ ($R^2 = 0.80$, $p < 0.001$). These results indicate that higher I_G values correspond to shorter inter-hillslope lag times, suggesting enhanced hydrological connectivity and transmissivity feedback mechanisms, as described in previous studies (Kendall et al., 1999; Bishop et al., 2011).

As peak I_G approaches 0.30, Δt converges to near-zero with minimal fluctuations, particularly during extreme storm events. This finding supports the results presented in Fig. 11, which demonstrate that elevated GWLs synchronize GWL responses across the watershed. This synchronization reflects a critical hydrological mechanism driven by transmissivity feedback, which amplifies groundwater movement, reduces lag times, and enhances watershed-scale connectivity. This dynamic is consistent with the work of Padilla et al. (2015), who reported that shorter lag times in bedrock aquifers with high-transmissivity conduits, and Scaife et al. (2020), who noted that increased connectivity during high GWL conditions reduces lag times and enhances watershed-scale hydrological responses.

Furthermore, although Fig. 12 labels the vertical axis as I_G to represent watershed-wide GWL status, a similar pattern emerges when replacing I_G with site specific GWL values, though the GWL

thresholds may vary among observation sites. These observations reinforce the idea that watershed-scale groundwater dynamics are influenced by the interplay between spatially variable geological conditions and temporal variations in GWL.

4.2 Delayed stormflow processes linked to GWL dynamics

~~## 4.1 Delayed stormflow processes dynamically aligned with GWL dynamics~~

Previous studies ~~(Cui et al., 2024) indicated~~ have shown that streamflow in XEW frequently exhibits a bimodal hydrograph during heavy rainfall~~, the streamflow in the XEW exhibits a bimodal hydrograph~~, with delayed stormflow likely originating~~formed by~~ from shallow groundwater outflow (Cui et al., 2024). Understanding~~Assessing~~ the ~~relative~~ timing and lag~~s~~ between groundwater and streamflow responses is crucial~~crucial~~ for identifying~~understanding~~ dominant runoff generation mechanisms~~processes~~ (Beiter et al., 2020). Discrepancies~~Inconsistencies~~ in these timings can indicate~~in response times may indicate the~~ contributions ~~of~~ from different~~alternative~~ water sources to the stream channel. Fig. 13 illustrates the relative timing of maximum I_G (I_{Gp}) and maximum SWC (SWC_p) ~~responses~~ for eight storm events, alongside~~as well as the~~ rainfall duration. ~~Each horizontal bar represents the onset of rain on the left end and the lag time for the maximum value on the right end of the corresponding variable, except that the bar length for t_{Rain} indicates the duration of the rainfall.~~

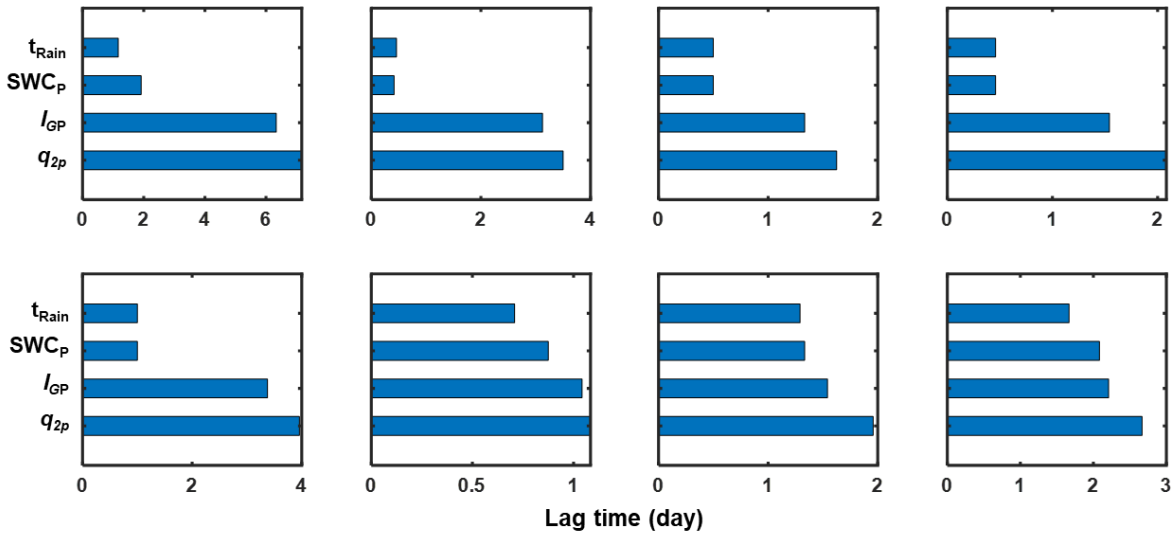

Figure 13. Lag times of maximum ~~soil water content~~SWC and ~~groundwater level~~GWL relative to rainfall onset. ~~The beginning and end of e~~Each ~~colored~~ bar indicates the rise and peak times of the ~~according~~ variable, with t_{Rain} indicating rainfall duration.~~.~~ SWC_{SP} and I_{GP} represent the~~is~~ maximum ~~soil water content~~SWC and~~. I_{GP} is the maximum~~ I_G~~,~~ respectively, while ~~and~~ q_{2p} denotes~~is~~ the delayed streamflow peak.

Rainfall durations for the analyzed ~~across~~ events ranged from 0.46 to 1.67 days. SWC, I_G, and delayed stormflow (q_{2p}) followed a clear sequence in their peak timings~~successively reached their peak values following~~ relative to rainfall ~~the~~ onset ~~of a storm~~. SWC responded rapidly ~~to rainfall~~, with its peak occurring 0.4 to 2.1 days after ~~the storm~~rainfall began, usually~~typically~~ coinciding with or slightly after rainfall cessation~~the end of the rainfall~~. In contrast, I_G continued to increase after the SWC peak~~,~~ and ~~reaching~~ reached its maximum before the ~~peak~~ delayed stormflow~~in~~ peak (q_{2p}). While ~~T~~the lag times between~~from the~~ SWC_p ~~to~~, ~~the~~ I_{Gp}, and q_{2p} varied ~~considerably across~~among events~~. However~~, the lag ~~time~~ between I_{Gp} and q_{2p} remained~~was~~ relatively consistent ~~across events~~.

This pattern aligns with findings~~As the prior research of~~ from Haught and Meerveld (2011) and Rinderer et al. (2016), who suggest~~reported~~ that when groundwater response precedes or synchronizes with streamflow,~~identical or earlier response timing of groundwater compared to streamflow implies~~ it indicates strong ~~that a robust~~ hillslope-stream connectivity, with groundwater serving as the primary driver of streamflow. ~~is established and the streamflow response is driven by hillslope groundwater.~~ Our results corroborate this view~~reinforce this understanding~~, showing that ~~as the~~q_{2p} timing ~~of q_{2p} was~~is predominantly governed by ~~changes in~~ groundwater dynamics. This relationship~~conclusion~~ is further validated~~corroborated~~ by the strong linear correlation between the lag times of q_{2p} (t_{2p}) and I_{Gp} (t_{IGp}), as indicated by the regression equation $t_{2p} = 1.11 \times t_{IGp} + 0.17$, with a slope of 1.11, showing a high~~a~~ determination coefficient ($R^2 = 0.995$~~, , and a t-test significance at the~~ $p <$ 0.01 ~~level~~). (Fig. 14).

Conversely,~~Conversely,~~ the correlation between t_{2p} and the lag time of SWC_p~~SWCp~~ (t_{SWCp}) was weak~~, with~~ ($R^2 = 0.029$ ~~and a t-test significance level of~~, $p =$ 0.688), ~~well above the 0.05 threshold,~~ indicating that the timing of SWC_p ~~t_{SWCp}~~ has ~~a negligible~~minimal influence ~~impact~~ on the delayed streamflow peak.~~ t_{2p}.~~ Additionally, ~~as shown in Fig. A1,~~ the I_G pattern~~process lines~~ during the delayed

stormflow period closely mirrored the shape of the streamflow hydrograph (Fig. A1), reinforcing the dominant role of I_G plays in controlling delayed stormflow~~further emphasizing the dominant role of I_G in controlling q_{2p}.~~

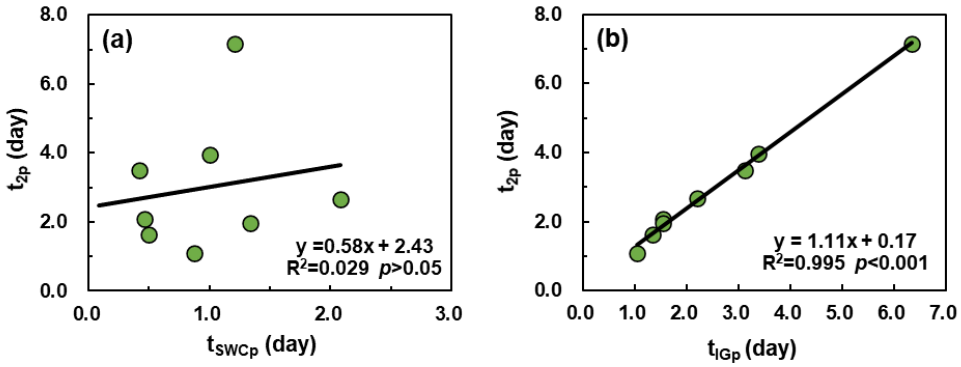

Figure 14. Lag times of maximum (a) SWC and (b) I_G ~~in~~ relative~~relation~~ to ~~the lag times of~~ delayed streamflow peaks (t_{2p}). t_{SWCp} and t_{IGp} denote~~are~~ the peak~~occurrence~~ times of the ~~maximum soil water content~~SWC and ~~maximum~~ I_G, respectively.

Further quantitative analysis revealed ~~The delayed stormflow process was quantitatively analyzed in relation to I_G variations during this phase~~a strong exponential relationship between streamflow and I_G during the delayed stormflow period~~. As shown in~~ (Fig. 15~~,~~). ~~during~~ In the ~~delayed stormflow period (i.e.,~~ non-rainfall ~~period)~~phase of the eight bimodal events, streamflow ~~demonstrated a strong exponential relationship with increases in~~increased exponentially with GWL (IG_p), exhibiting~~with~~ a highly significant correlation ($p < 0.001$) and a determination~~correlation~~ coefficient of $R^2 = 0.90$. This exponential increase~~rise~~ in streamflow is attributed to the increase in lateral hydraulic conductivity as the water table approaches the surface~~corresponding to the increase in GWL can be attributed to a potential enhancement in lateral hydraulic conductivity as the water table approaches the land surface,~~. Similar findings have been reported by~~consistent with findings by~~ Detty and McGuire (2010) and Kendall et al. (1999), where groundwater outflow dominates during storm events.~~.~~

~~Furthermore, the rapid increase in streamflow as the water table enters the surficial zone flattens the GWL vs. streamflow curve, indicating the occurrence of transmissivity feedback. This feedback mechanism led to a rise in GWL, which mobilized groundwater outflow, facilitating rapid transport~~

~~via shallow flow paths to the stream, as described by Lundin (1982).~~

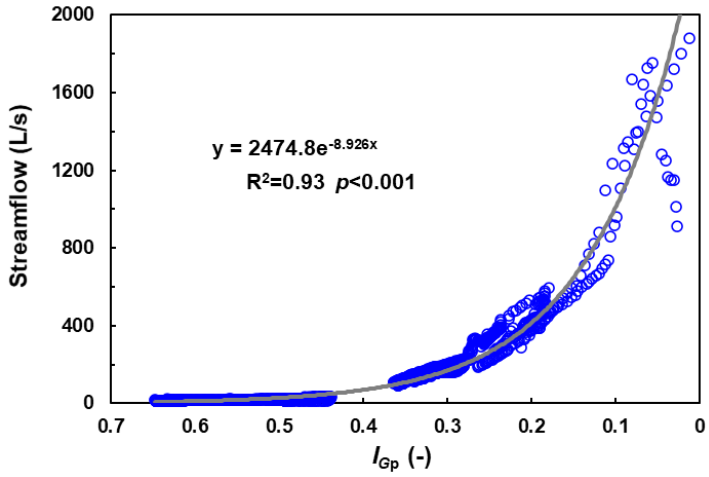

Figure 15. Correlation between I_G and streamflow during delayed stormflow periods.

At higher GWLs, the curve of GWL vs. streamflow begins to flatten, suggesting a feedback mechanism. As the rising water table mobilizes shallow groundwater outflow, water is rapidly transported to the stream via shallow flow paths. This process, often referred to as transmissivity feedback, is consistent with Lundin's (1982) description of groundwater dynamics during delayed stormflow periods.

4.3 Delayed stormflow processes linked to GWL dynamics

Understanding the critical~~activation~~ thresholds that govern the movement of water within landscape~~movement is~~ is ~~crucial~~essential for accurately predicting delayed stormflow, as emphasized by McDonnell et al. (2021). ~~Previous analyses in t~~This study identified a strong Relationship ~~correlation~~ between delayed stormflow and the gradual~~slow~~ response of GWL, primarily~~. This slow response is~~ influenced~~triggered~~ by a sharp~~rapid~~ decline in SWC when it exceeds~~, which only occurs when SWC exceeds~~ a critical threshold of 0.20.

To identify ~~pinpoint~~ the ~~control~~ threshold for delayed stormflow initiation in XEW, we analyzed 63 out of 95 rainfall-runoff events ~~that had~~with complete ~~SWC and GWL~~streamflow data. The relationship between SWCp and q_s for these events is illustrated ~~illustrated~~ in Fig. 16. A clear~~distinct~~ threshold behavior~~phenomenon~~ emerged~~was observed~~: when SWC was below 0.20, q_s remained

minimal ~~when SWC was below 0.20, consistent with a condition prevalent in nearly all~~ unimodal events. However, as ~~when~~ SWC exceeded~~surpassed~~ 0.20, a noticeable~~there was a sudden~~ increase in q_s was observed, signaling the onset~~due to the emergence~~ of delayed stormflow in some events. Specifically,~~Notably,~~ when SWC surpassed~~exceeded~~ 0.23, a pronounced~~significant~~ surge in stormflow volume occurred~~occurred~~, accompanied by the emergence of~~with~~ a secondary stormflow peak ~~appearing~~ in all events. ~~This~~ These findings suggest~~s~~ that ~~an SWC range of 0.20 to 0.23 reflects~~ the ~~soil layer's water storage capacity, serving as a~~ critical threshold for ~~the onset of~~ delayed stormflow initiation lies within the SWC range of 0.20 to 0.23.

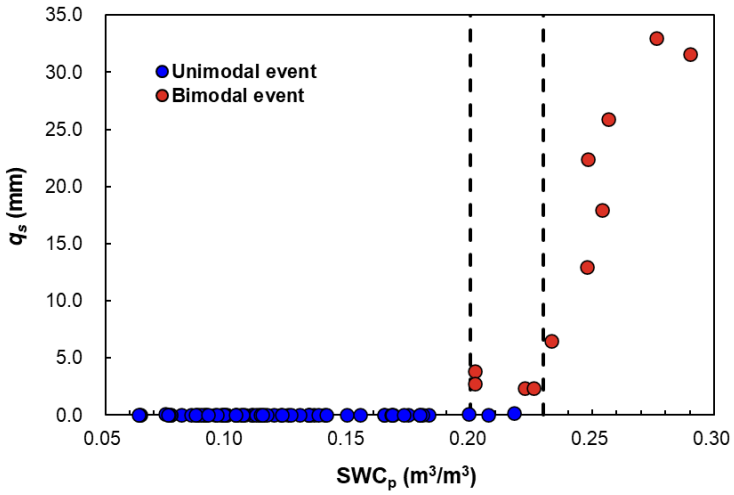

Figure 16. Relationship between maximum ~~soil water content~~SWC (SWC_p) and event stormflow ~~amount~~ volume (q_s).

These results~~findings~~ underscore~~highlight~~ the pivotal role of the surface soil layer's water deficit or water-holding capacity in triggering~~determining the rainfall threshold for~~ delayed stormflow ~~initiation~~. During rainfall events, the soil retains water until its water-holding capacity is exceeded~~rainwater was largely retained within the soil layer until the amount exceeded its water-holding capacity~~. Once SWC surpasses the threshold of 0.20, the soil begins to release water more rapidly, initiating delayed stormflow. Additionally~~Furthermore~~, ~~the analysis revealed that~~ during unimodal events, stormflow (q_s) remained consistently below 1 mm despite variations in SWC,~~despite fluctuations in SWC, the q_s generated during unimodal events consistently remained below 1 mm,~~ indicating that stormflow in these cases arises~~was mainly due to~~ mainly from direct

rainfall interception by the channel rather than delayed soil water release.

While the depth and distribution of soil layers likely influence the watershed's overall ~~Given the varying soil layer depths across the watershed, more detailed data on soil depth and distribution are essential for accurately estimating watershed-wide soil~~ water storage capacity~~.~~, observed SWC data showed minimal spatial variability across locations ~~However, observations of SWC across different locations~~ within the watershed.~~show minimal variability within the watershed,~~ This suggest~~s~~ing that SWC ~~serves as~~can reliably represent ~~a reliable indicator of~~ the watershed's overall soil water storage capacity~~in this study~~.

One limitation of this study lies in the indirect estimation of field capacity through observed SWC thresholds rather than direct measurement or modeling. Although this approach aligns with observed patterns and simplifies the analysis, it does not fully capture the spatial variability of field capacity or its dependence on soil depth. Future work should incorporate direct field capacity measurements or modeling to refine the relationship between SWC and delayed stormflow initiation, thereby improving the accuracy of threshold predictions.

~~4.1~~4.4 Conceptual model of runoff generation in XEW

~~In t~~This section~~, we~~ present~~s~~ a conceptual model ~~that~~ elucidate~~s~~ing the runoff generation mechanisms ~~of runoff generation~~ in ~~the~~ XEW ~~watershed~~, with a particular focus on the interplay between ~~role of~~ soil water storage and GWL dynamics. Soil water storage is identified as the critical factor driving the transition from initial to delayed runoff generation. Once the soil water deficit is replenished, the slowly rising GWL becomes the dominant~~primary~~ control ~~on~~ in the delayed stormflow process. Fig 17 illustrates the conceptual framework,~~model of runoff generation,~~ which incorporates transmissivity feedback mechanisms to explain the formation of distinct hydrograph~~s~~ patterns.

1. **Runoff generation under dry conditions (Fig. 17b):**

In dry watershed conditions, characterized by low antecedent moisture and light rainfall,~~When~~

~~the watershed is relatively dry and experiences light rainfall, the model shows that~~ rainwater primarily infiltrates and is retained ~~stored within~~in the soil ~~layer~~profiles. Streamflow ~~During~~ during such events consists~~, the streamflow is composed~~ of two primary~~main~~ components: (1) a rapid yet modest streamflow peak driven by~~resulting from~~ direct rainfall onto the channel and (2) a relatively stable baseflow originating from the gradual release of deep groundwater reservoirs.

Under these conditions, the baseflow reflects the slow release of groundwater stored in deeper aquifers, while the limited rainfall input is insufficient to trigger significant connectivity between hillslopes and the channel.~~This baseflow contribution is relatively constant, reflecting the slow discharge of groundwater from deeper aquifers.~~

2. Delayed stormflow during moderate storms (Fig. 17c):

As rainfall intensity and duration increase, moderate storm events lead to the replenishment of soil water deficits, resulting in the exceedance of soil storage capacity. Initially, the response resembles that of dry conditions, with a rapid streamflow peak generated by direct channel rainfall. However, as rainfall continues, excess water infiltrates deeper, elevating the GWL and expanding the saturated zone.

~~In more substantial storm events, the soil water storage capacity is exceeded after the soil water deficit is fully replenished. The initial response is similar to the dry condition scenario, with a rapid streamflow peak generated by direct rainfall on the channel. However, as rainfall continues, the excess water infiltrates deeply, elevating the GWL and expanding the effective connection area between the stream channel and adjacent hillslopes. T~~This process enhances the hydraulic connectivity between the stream channel and adjacent hillslopes, facilitating the lateral transport of shallow groundwater to the channel. As the GWL intersects more conductive soil layers, a delayed stormflow peak is observed, typically occurring after rainfall ceases. This secondary peak reflects the combined effects of deep infiltration, gradual GWL rise, and increased transmissivity in the subsurface, which accelerates shallow groundwater movement towards the channel.~~his vertical expansion of the saturated zone allows a significant volume of shallow groundwater to be rapidly conveyed to the channel as the~~

~~GWL reaches a more conductive soil layer. The result is a delayed stormflow peak, which occurs after the rainfall has ended.~~

3. Runoff generation during extreme storm events (Fig. 17d):

Extreme storm events, characterized by high rainfall intensity and large volumes, result in a sharp and widespread rise in GWL across the entire watershed. During such events, the rapid expansion of saturated areas and the increased hydraulic conductivity of the subsurface enable the swift mobilization of shallow groundwater. This synchronous response generates a pronounced flood peak within a short timeframe.

~~In extreme storm events characterized by substantial rainfall input, GWLs rise sharply across the entire watershed, reaching levels associated with higher hydraulic conductivity. This synchronous rise in GWL triggers the rapid release of a large volume of shallow groundwater, leading to a significant flood peak within a short time frame.~~ In the riparian zones, GWLs may rise into the soil profile or even reach the ground surface, facilitating direct water flow into the channel via subsurface pathways. Observational data from extreme events corroborate this mechanism, as significant increases in SWC are recorded in the deeper soil layers of riparian zones after rainfall ends. This pattern suggests that groundwater from adjacent hillslopes contributes to the replenishment of soil water in these zones, reinforcing lateral subsurface flow pathways. ~~During these events, the GWL in the riparian zone may rise into the soil layer or even reach the ground surface, facilitating water movement into the channel via soil subsurface flow. Observations from extreme storm events support this mechanism, as the deeper soil layer in the riparian zones often shows a sudden and sustained increase in SWC after rainfall has ceased, suggesting that groundwater from adjacent hillslopes may be replenishing soil water in these areas.~~

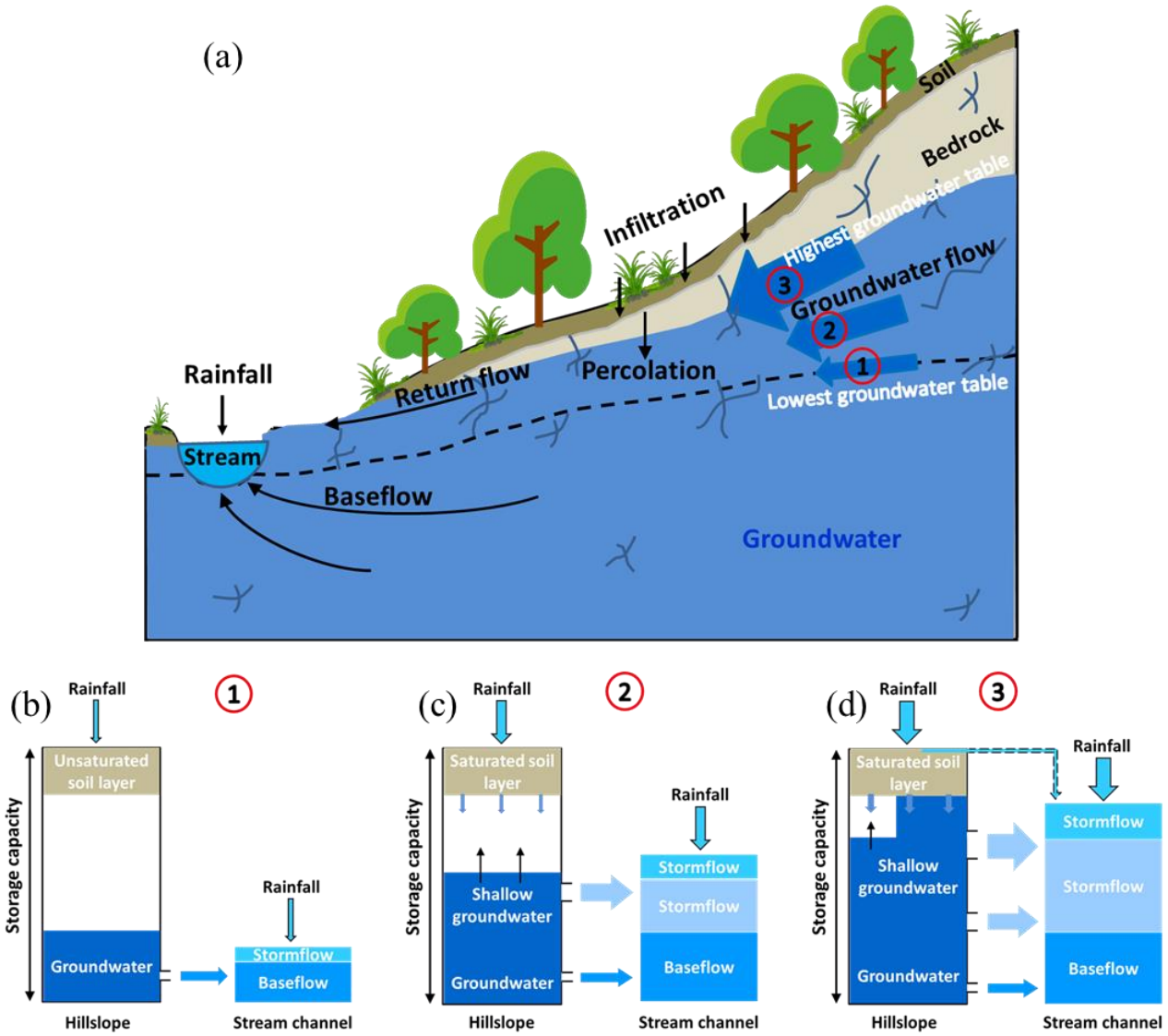

Figure 17. Conceptual model illustrating ~~the~~ stormflow generation associated with the transmissivity feedback.

The progression~~transition~~ from the runoff generation ~~model~~ under dry conditions (~~depicted in~~ Fig. 17b) to moderate storm scenarios (Fig. 17c) and ultimately extreme events (Fig. 17d) reflects the~~corresponds to a~~ progressive wetting-up of the watershed. ~~The a~~Abrupt changes in stormflow volume and timing are initially ~~t~~governed ~~riggered~~ by soil water storage thresholds and subsequently controlled~~later governed~~ by the hydraulic conductivity of the bedrock and micro-topography.

This conceptual model provides a quantitative framework for understanding how variations in~~varying~~ hydrological conditions influence ~~the~~ runoff generation processes in ~~the~~ XEW ~~watershed~~.

By integrating soil water storage dynamics, GWL responses, and transmissivity feedback mechanisms, the model offers insights into the nonlinear behavior of runoff processes under different rainfall scenarios.

5. Conclusions

Building upon previous work that identified and characterized bimodal streamflow patterns in ~~the~~ XEW ~~watershed~~, this study ~~provides a detailed,~~ quantitatively ~~analysis~~ analyzed ~~of~~ SWC and GWL dynamics at the event scale to elucidate the mechanisms driving ~~behind~~ delayed stormflow generation. The findings reveal that when soil water storage surpasses its holding capacity, a secondary increase in streamflow is triggered. This secondary, or delayed, stormflow is primarily governed by GWL dynamics, which dictate~~influencing~~ both the magnitude of the delayed ~~stormflow~~ response and the lag time to its peak.

During rainfall events, SWC responds rapidly,~~exhibits a rapid response, continuing to~~ increase~~ing~~ until the soil's water storage capacity ~~it~~ is ~~reaches~~ reached or ~~exceeds~~exceeded ~~the soil's water storage capacity~~. If the stored water remains within this capacity, SWC stabilizes or decreases gradually~~slowly~~ following the cessation of ~~after~~ rainfall ~~ceases~~, eventually leveling off near the field capacity. The rate of this ~~SWC~~ decrease is closely linked~~directly proportional~~ to the extent of SWC ~~to which it~~ exceed~~s~~ing the field capacity. When SWC begins to decline~~decreases~~, excess rainwater percolates~~infiltrates~~ deeper into the soil, raising the GWL. Once ~~the~~ GWL begins to rise, it becomes the dominant driver ~~factor driving~~of the delayed stormflow process.

As GWL rises, hydraulic conductivity increases, facilitating enhanced~~allowing more~~ groundwater ~~to flow~~flux from hillslopes ~~into~~ to the stream channel~~, thereby forming delayed stormflow~~. This process expands~~also causes~~ the effective connectivity~~connection area~~ between the ~~stream~~ channel and adjacent hillslopes ~~to expand vertically~~. At specific high GWL thresholds, the synchronization of GWL responses across multiple hillslopes significantly amplifies~~leads to a substantial increase in~~ stormflow volume. This synchronized response shortens the lag time and increases the volume of delayed stormflow, often merging~~causing~~ the delayed ~~stormflow~~ peak ~~to~~

~~merge~~ with the direct stormflow peak.

These findings offer~~provide~~ critical insights into~~a deeper understanding of~~ the nonlinear processes governing stormflow generation and~~behavior of stormflow and the mechanisms behind~~ the formation of bimodal hydrographs. ~~T~~By elucidating the mechanisms underpinning these dynamics, the study advances hydrological theory and provides actionable knowledge for improving flood modeling and prediction.~~his enhanced understanding has significant implications for advancing hydrological theory and offers valuable insights for improving and optimizing flood modeling and prediction.~~

Data availability

The data supporting this study are available on the Zenodo website at https://doi.org/10.5281/zenodo.12581739.~~All the data used in this study will be available at the Zenodo website at the time of publication.~~

Author contribution

ZC contributed the conceptualization, formal analysis, investigation and writing; FT contributed the conceptualization, formal analysis and revision.

Competing interests

Fuqiang Tian is a member~~s~~ of the editorial board of Hydrology and Earth System Sciences.

Acknowledgements

This study was supported by National Key R&D Program of China (2022YFC3002902) and National Natural Science Foundation of China (51825902).

5. References

Ali, G., Oswald, C. J., Spence, C., Cammeraat, E. L., McGuire, K. J., Meixner, T., and Reaney, S. M.: Towards a unified threshold-based hydrological theory: necessary components and recurring challenges, Hydrol. Process., 27, 313–318, https://doi.org/10.1002/hyp.9560, 2013.

Anderson, M. G., and Burt, T. R.: The role of topography in controlling throughflow generation, Earth Surf. Process., 3, 331–334, https://doi.org/10.1002/esp.3290030402, 1978.

Beiter, D., Weiler, M., and Blume, T.: Characterising hillslope–stream connectivity with a joint event analysis of stream and groundwater levels, Hydrol. Earth Syst. Sci., 24, 5713-5744, https://doi.org/10.5194/hess-24-5713-2020, 2020.

Bishop, K., Seibert, J., Nyberg, L., and Rodhe, A.: Water storage in a till catchment. II: Implications of transmissivity feedback for flow paths and turnover times, Hydrol. Process., 25, 3950-3959, https://doi.org/10.1002/hyp.8355, 2011.

Cain, M. R., Woo, D. K., Kumar, P., Keefer, L., and Ward, A. S.: Antecedent conditions control thresholds of tile-runoff generation and nitrogen export in intensively managed landscapes, Water Resour. Res., 58, e2021WR030507, https://doi.org/10.1029/2021WR030507, 2022.

Cui, Z., Tian, F., Zhao, Z., Xu, Z., Duan, Y., Wen, J., and Khan, M. Y. A.: Bimodal Hydrographs in Semi-humid Forested Watershed: Characteristics and Occurrence Conditions, Hydrol. Earth Syst. Sci. Discuss., https://doi.org/10.5194/hess-2024-36, 2024.

Dang, L., Xie, Y. Q., Wang, C., Chang, Y., Zeng, X. K., and Wu, J. C.: Precipitation-induced Pressure Wave Propagation in Unsaturated Zone and Its Effect on Rapid Groundwater Discharge, Geol. J. China Univ., 29, 580-589, https://doi.org/10.16108/j.issn1006-7493.2021104, 2023.

Detty, J. M., and McGuire, K. J.: Threshold changes in storm runoff generation at a till-mantled headwater catchment, Water Resour. Res., 46, W07525, https://doi.org/10.1029/2009WR008102, 2010.

Farrick, K. K., and Branfireun, B. A.: Soil water storage, rainfall and runoff relationships in a tropical dry forest catchment, Water Resour. Res., 50, 9236-9250, https://doi.org/10.1002/2014WR016045, 2014.

Fu, C., Chen, J., Jiang, H., and Dong, L.: Threshold behavior in a fissured granitic catchment in southern China: 1. Analysis of field monitoring results, Water Resour. Res., 49, 2519-2535, https://doi.org/10.1002/wrcr.20193, 2013.

Graeff, T., Zehe, E., Reusser, D., Lück, E., Schröder, B., Wenk, G., John, H., and Bronstert, A.: Process identification through rejection of model structures in a mid-mountainous rural catchment: observations of rainfall-runoff response, geophysical conditions and model inter-comparison, Hydrol. Process., 23, 702–718, https://doi.org/10.1002/hyp.7171, 2009.

Graham, C. B., and McDonnell, J. J.: Hillslope threshold response to rainfall: (2) development and use of a macroscale model, J. Hydrol., 393, 77–93, https://doi.org/10.1016/j.jhydrol.2010.03.008, 2010.

Graham, C. B., Woods, R. A., and McDonnell, J. J.: Hillslope threshold response to rainfall: (1) A field based forensic approach, J. Hydrol., 393, 65–76, https://doi.org/10.1016/j.jhydrol.2009.12.015, 2010.

Haga, H., Matsumoto, Y., Matsutani, J., Fujita, M., Nishida, K., and Sakamoto, Y.: Flow paths, rainfall properties, and antecedent soil moisture controlling lags to peak discharge in a granitic unchanneled catchment, Water Resour. Res., 41, W2179–W2187, https://doi.org/10.1029/2005wr004236, 2005.

Haught, D. R. W. and Meerveld, H. J.: Spatial variation in transient water table responses: differences between an upper and lower hillslope zone, Hydrol. Process., 25, 3866-3877, https://doi.org/10.1002/hyp.8354, 2011.

Hewlett, J. D., and Hibbert, A. R.: Factors affecting the response of small watersheds to precipitation in humid areas, in: Forest Hydrology, edited by: Sopper, W. E. and Lull, H. W., Pergamon Press, Oxford, 275–290, 1967.

Jin, Z., Guo, L., Yu, Y., Luo, D., Fan, B., and Chu, G.: Storm runoff generation in headwater catchments on the Chinese Loess Plateau after long-term vegetation rehabilitation, Sci. Total Environ., 748, 141375, https://doi.org/10.1016/j.scitotenv.2020.141375, 2020.

Kendall, K. A., Shanley, J. B., and McDonnell, J. J.: A hydrometric and geochemical approach to test the transmissivity feedback hypothesis during snowmelt, J. Hydrol., 219, 188–205, https://doi.org/10.1016/S0022-1694(99)00059-1, 1999.

Kosugi, K., Fujimoto, M., Katsura, S., Kato, H., Sando, Y., and Mizuyama, T.: Localized bedrock aquifer distribution explains discharge from a headwater catchment, Water Resour. Res., 47, W07111, https://doi.org/10.1029/2010WR009884, 2011.

Martínez-Carreras, N., Hissler, C., Gourdol, L., Klaus, J., Juilleret, J., Iffly, J. F., and Pfister, L.: Storage controls on the generation of double peak hydrographs in a forested headwater catchment, J. Hydrol., 543, 255–269, https://doi.org/10.1016/j.jhydrol.2016.10.004, 2016.

McDonnell, J. J., Spence, C., Karran, D. J., Van Meerveld, H. J., and Harman, C. J.: Fill-and-spill: A process description of runoff generation at the scale of the beholder, Water Resour. Res., 57, e2020WR027514, https://doi.org/10.1029/2020WR027514, 2021.

McGuire, K. J., and McDonnell, J. J.: Hydrological connectivity of hillslopes and streams: characteristic time scales and nonlinearities, Water Resour. Res., 46, W10530, https://doi.org/10.1029/2010WR009341, 2010.

Padilla, C., Onda, Y., and Iida, T.: Interaction between runoff–bedrock groundwater in a steep headwater catchment underlain by sedimentary bedrock fractured by gravitational deformation, Hydrol. Process., 29, 4398–4412, https://doi.org/10.1002/hyp.10498, 2015.

Penna, D., Tromp-van Meerveld, H. J., Gobbi, A., Borga, M., and Dalla Fontana, G.: The influence of soil moisture on threshold runoff generation processes in an alpine headwater catchment, Hydrol. Earth Syst. Sci., 15, 689-702, https://doi.org/10.5194/hess-15-689-2011, 2011.

Phillips, J. D.: Sources of nonlinearity and complexity in geomorphic systems, Prog. Phys. Geogr., 27, 1-23, https://doi.org/10.1191/0309133303pp340ra, 2003.

Rinderer, M., van Meerveld, I., Stähli, M., and Seibert, J.: Is groundwater response timing in a pre-alpine catchment controlled more by topography or by rainfall? Hydrol. Process., 30, 1036-1051, https://doi.org/10.1002/hyp.10634, 2016.

Ross, C. A., Ali, G. A., Spence, C., and Courchesne, F.: Evaluating the Ubiquity of Thresholds in Rainfall - Runoff

Response Across Contrasting Environments, Water Resour. Res., 57, e2020WR027498, https://doi.org/10.1029/2020WR027498, 2021.

Sakakibara, K., and Suzuki, K.: Controlling Factors and Characteristics of Peak Runoff in an Alpine Headwater Under the Asian Monsoon Climate, Mt. Res. Dev., 42, R1–R8, https://doi.org/10.1659/MRD-JOURNAL-D-21-00030.1, 2022.

Scaife, C. I., and Band, L. E.: Nonstationarity in threshold response of stormflow in southern Appalachian headwater catchments, Water Resour. Res., 53, 6579-6596, https://doi.org/10.1002/2017WR020376, 2017.

Scaife, C. I., Singh, N. K., Emanuel, R. E., Miniat, C. F., and Band, L. E.: Non-linear quickflow response as indicators of runoff generation mechanisms, Hydrol. Process., 34, 2949–2964, https://doi.org/10.1002/hyp.13780, 2020.

Sivapalan, M.: Process complexity at hillslope scale, process simplicity at watershed scale: Is there a connection, Hydrol. Process., 17, 1037-1041, https://doi.org/10.1002/wrcr.20193, 2003.

Sloto, R. A., and Crouse, M. Y.: HYSEP: A computer program for streamflow hydrograph separation and analysis, US Geol. Surv., https://doi.org/10.3133/wri964040, 1996.

Tian, F., Li, H., and Sivapalan, M.: Model diagnostic analysis of seasonal switching of runoff generation mechanisms in the blue river basin, Oklahoma, J. Hydrol., 418-419, 136–149, https://doi.org/10.1016/j.jhydrol.2010.03.011, 2012.

Tie, Q., Hu, H., Tian, F., and Holbrook, N. M.: Comparing different methods for determining forest evapotranspiration and its components at multiple temporal scales, Sci. Total Environ., 633, 12–29, https://doi.org/10.1016/j.scitotenv.2018.03.082, 2018.

Tromp-van Meerveld, H. J., and McDonnell, J. J.: Threshold relations in subsurface stormflow: 1. A 147-storm analysis of the Panola hillslope, Water Resour. Res., 42, W02410, https://doi.org/10.1029/2004WR003778, 2006a.

Tromp-van Meerveld, H. J., and McDonnell, J. J.: Threshold relations in subsurface stormflow: 2. The fill and spill hypothesis, Water Resour. Res., 42, W02411, https://doi.org/10.1029/2004WR003800, 2006b.

Uchida, T., Tromp-van Meerveld, I., and McDonnell, J. J.: The role of lateral pipe flow in hillslope runoff response: an intercomparison of non-linear hillslope response, J. Hydrol., 311, 117-133, https://doi.org/10.1016/j.jhydrol.2005.01.012, 2005.

Zhang, G., Cui, P., Gualtieri, C., Zhang, J., Bazai, N. A., Zhang, Z., Wang, J., Tang, J. B., Chen, R., and Lei, M.: Stormflow generation in a humid forest watershed controlled by antecedent wetness and rainfall amounts, J. Hydrol., 603, 127107, https://doi.org/10.1016/j.jhydrol.2021.127107, 2021.

Appendix A:

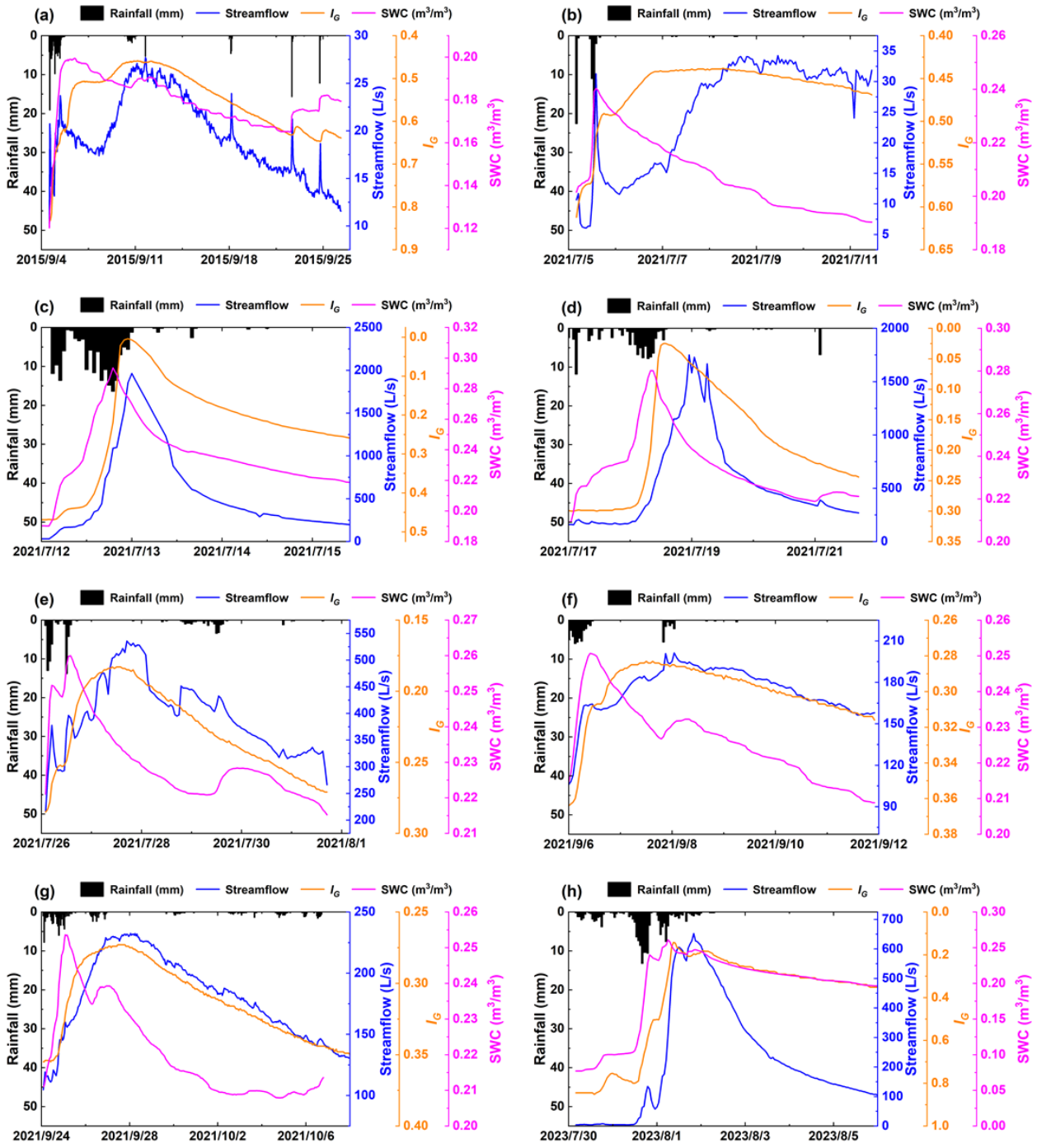

Figure A1. Examples of responses of streamflow, IG and soil water content to rainfall.